

Article

The Influence of Regional Groundwater Flow and a Neighbouring River on the Behaviour of an Aquifer Thermal Energy Storage System

Qais H. M. Al-Madhloom ^{1,*} , Sanaa A. Jassim ² and Riyadh H. M. Muttaleb ³

¹ Department of Automobile Engineering, Faculty of Engineering/Al-Musayab, University of Babylon, Hilla 51002, Iraq

² Department of Energy & Renewable Energy Engineering, Faculty of Engineering/Al-Musayab, University of Babylon, Hilla 51002, Iraq; met.sanaa.abd@uobabylon.edu.iq

³ Department of Civil Engineering, Faculty of Engineering, University of Babylon, Hilla 51002, Iraq; eng.riyadh.mohammed@uobabylon.edu.iq

* Correspondence: met.qais.hatem@uobabylon.edu.iq or qais.alsaady@gmail.com

Abstract: One promising solution for mitigating CO₂ emissions in arid regions is to use Aquifer Thermal Energy Storage (ATES) systems in cooling and heating systems. However, ATES systems need to be subjected to geohydrological investigations before their installation to ensure high performance. Two geohydrological properties are considered: regional groundwater flow and the influence of neighbouring rivers. This study considers a hypothetical ATES system within the city of Hilla, Iraq. MODFLOW 6.1 software was used to simulate the influence of the two properties. The simulation tested two locations situated at 75 m and 300 m from the river. Each location was explored using three flow rates: 10 m³/d, 50 m³/d, and 100 m³/d. The results indicate that the temperature change in the warm and cold wells increases proportionally with time of operation and rate of flow. For example, the temperature of the middle layer (for 10 m³/d operation) changes from 29 °C (after one year) to 34 °C (after twenty years operation), while it changes from 34 °C (one year) to 35 °C (twenty years) under 100 m³/d operation. Another result is that the available regional groundwater flow has a negligible influence on the storage system, while the neighbouring river has a high influence on the stored energy when the distance between them is 75 m or less. The paper recommends the installation of ATES systems at least 300 m from the bank of a river.

Keywords: aquifer thermal energy storage system; regional groundwater flow; neighbouring rivers; simulation using MODFLOW Flex; arid climate



Citation: Al-Madhloom, Q.H.M.; Jassim, S.A.; Muttaleb, R.H.M. The Influence of Regional Groundwater Flow and a Neighbouring River on the Behaviour of an Aquifer Thermal Energy Storage System. *Water* **2024**, *16*, 548. <https://doi.org/10.3390/w16040548>

Academic Editors: Jun Song Kim, Dong-Kyun Kim and Donghae Baek

Received: 1 January 2024

Revised: 30 January 2024

Accepted: 5 February 2024

Published: 9 February 2024



Copyright: © 2024 by the authors. Licensee MDPI, Basel, Switzerland. This article is an open access article distributed under the terms and conditions of the Creative Commons Attribution (CC BY) license (<https://creativecommons.org/licenses/by/4.0/>).

1. Introduction

One of the biggest challenges that has faced humankind in recent decades is greenhouse gases, or CO₂ emissions. During the last 320,000 years, the atmospheric CO₂ concentration did not exceed 300 ppm, with the normal CO₂ concentration being between 280 ppm and 350 ppm [1]. Now, however, it has increased to 418 ppm [1], mainly due to the enormous quantity of CO₂ emissions that the world produces. The global heating and cooling demand contributes to CO₂ emissions. Fortunately, with an increased knowledge of the problem, there is now more awareness of the risks that face life on earth, both currently and for future generations. Global efforts have been made to decrease the dangerous development of this problem. Electricity producers are responsible for 682 Mt per year [2]. The residential sector of Iraq, a Middle Eastern country, consumed about 92,062 TJ of electricity (about 57% of the nation's total electricity consumption) in 2019 [2]. Approximately three quarters of this value is consumed by conventional cooling and heating systems [3]. Iraq produced 174.56 Mt of CO₂ during 2019 [4]. Thus, controlling the world's heating and cooling sectors, particularly in arid countries such as Iraq, could be a key contribution to the global effort of minimizing the CO₂ problem [5].

One environmentally friendly solution that can mitigate the problems caused by conventional heating and cooling systems is the Aquifer Thermal Energy Storage (ATES) system [6–8]. This technology uses groundwater as thermal storage. It is intended to operate as a bridge for the seasonal mismatch that occurs between the available supply of and demand for cooling and heating energy supplied to buildings [9–12].

A typical ATES system consists of two wells (or groups of wells): warm and cold wells. In the summer, water is extracted from the cold well, circulated within the building or facility, and then reinjected into the warm well. During this process, the building or facility will be cooled. In the winter, the process is reversed, producing heat for the facility. Hot water is extracted from the warm well and used to heat the building. During this process, the water is cooled. Then, it is reinjected into the cold well to be stored and used the next summer [11,13,14]. In this process, a thermal balance in terms of the amount of heat extracted and reinjected into the ground is required to keep the system from collapsing due to thermal loads [8]. In cold regions, the cooling process in the summer is direct, while a heat pump is used to boost the heating in winter. The reverse is the case in hot regions, since the heat pump is utilized to activate the cooling process [11,15].

There are many factors behind the success of these systems, such as their high heat capacity and the low thermal conductivity of water, massive storage capacities, their high feasibility for implementation around the world, and low construction costs and payback times. All these factors make ATES systems eligible for use in large-scale applications such as hospitals, airports, universities, and district heating networks. Consequently, up until 2018, there had been 2800 successfully implemented ATES systems worldwide [6,7,10,11]. According to Schmidt et al. (2018), about 100 of these ATES systems are large-scale systems integrated with district heating and cooling (DH/DC) networks [16]. Most of these systems have been adopted in the Netherlands, which has suitable underground conditions, such as predominantly homogeneous aquifers with slow regional groundwater velocities [7]. One of the first of these systems is in Rostock, Germany. This system went into operation in 2000, and it supplies 108 apartments (7000 m² total living area) with district heating and domestic hot water. It reached its target, halving the total heat demand every year, after three years of operation [8].

However, although there are many advantages to ATES systems, they do have inherent drawbacks. For example, they require the presence of an aquifer which has suitable hydrogeological conditions, such as a low groundwater flow, high permeabilities, and the geochemical conditions that prevent the clogging and corrosion of wells [10]. Given this fact, many countries impose a set of conditions (restrictions) on ATES systems. For instance, the Netherlands sets two main restrictions. The first relates to the temperature of the injected water, which is not allowed to be more than 30 °C. The second restriction states that a thermal imbalance between hot and cold wells is not allowed [8,17].

The environmental influence of ATES depends on the groundwater conditions and aquifer sediments [18]. The environmental impact of ATES systems can be classified into four groups: hydrological; thermal; chemical; and microbiological [19]. The hydrological impact involves changing water levels and fluxes; changing other wells' capture zones; and poorly sealed boreholes, while the thermal influence presents changing water temperatures. The chemical impact describes mixing processes and chemical reactions; the reactivation of otherwise stable groundwater pollution plumes; the oxidation of organic matter; the oxidation of iron sulphides; the dissolution and precipitation of carbonates; the dissolution/precipitation of silicates; leaching from installation materials; and anti-freeze fluid or additive leaking. Finally, the microbiological impact includes the introduction or mobilization of pathogens; increasing biodegradation rates; and changing microbiological populations [19].

In Iraq, the conventional air to air heat pumps (e.g., windows and air conditioning) exhibits a large number of deficiencies in the summer. First, they are inefficient for cooling purposes because they have a low Coefficient of Performance (COP) since the outside air temperature is high (more than 50 °C). Second, performance is highly affected by dust

since the condenser efficiency decreases due to increasing thermal resistance. Thus, the heat transfer process will be slower compared to that of ATEs systems because the sink is the groundwater, which has a temperature of around 24 °C. The low performance of the conventional air conditioner is reflected in electricity demand, increasing it exponentially. In the winter season, heating systems still have the same problems, but to a lesser degree.

In spite of all the advantages of ATEs systems, no such systems have been built in Iraq. Furthermore, there are no studies considering the use of these systems in the country. The simulation of these systems is also seldom considered in studies, and this also holds true for the operation of ATEs systems under shallow water table conditions.

This study aimed to simulate the use of an ATEs system in shallow water table conditions within arid regions. In addition, it aims to explore how the stored energy spreads in the storage aquifer. This study will be very useful for the planning of new storage systems. In addition, this study aimed to determine the influence of the available regional groundwater flow and neighbouring rivers on the stored energy. The influence of such factors is important in terms of site selection for future ATEs systems. To achieve the aims of this study, we selected Babylon Province, in the middle of Iraq, as the study area. This study intends to answer the following questions: How does the stored energy spread in the considered storage aquifer? Does the present ambient groundwater flow affect the stored energy? Do neighbouring rivers affect the stored energy, and if so, to what extent? How does a neighbouring river affect the storage system when the distances between them are 75 m and 300 m?

2. Materials and Methods

This study involved a 3D simulation of a hypothetical ATEs system in operation within Babylon Province (Figure 1a,b). It was assumed that the ATEs system is installed within two different locations relative to the Shatt Al-Hilla River: 75 m and 300 m (Figure 1b). Furthermore, the simulation considered three different scenarios of operation in each location: 10, 50, and 100 m³/day. Thus, a total of six scenarios were considered in this study.

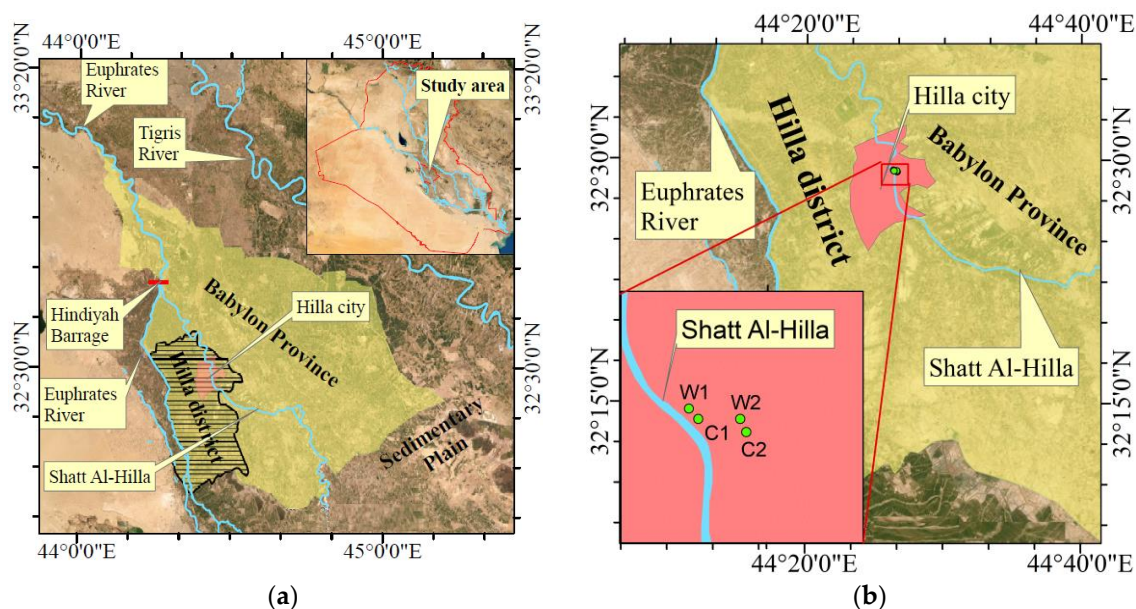


Figure 1. (a) The study area (Babylon Province); (b) the wells of the systems (W and C refer to the warm and cold wells, and the index refers to the number of ATEs systems).

2.1. Study Area

Although the method used here can be applied to any region, we used the of Hilla (the capital of Babylon Province) as our study area. Babylon Province is delimited by the

longitudes $44^{\circ}2'42''$ E and $45^{\circ}12'1''$ E and the latitudes $32^{\circ}5'54''$ N and $33^{\circ}7'35''$ N. Its area is about 5135 Km^2 (Figure 1a,b). Its population is about 2 million people [20].

There are two reasons for why we selected the city of Hilla, both of which are primarily based on the unusual conditions in this province: its shallow water table (Section 2.3) and its arid climate (Section 2.4).

2.2. Geological Conditions

The study area is part of the Sedimentary Plain of Iraq (see Figure 2). Its elevation ranges between 72 m.a.s.l. in the north and 11 m.a.s.l. in the south. This generally produces a ground surface slope less than 20 m/km [20–22]. The study area is covered by fluvial medium- and fine-grained sediments which range between clay and sand [21,22].

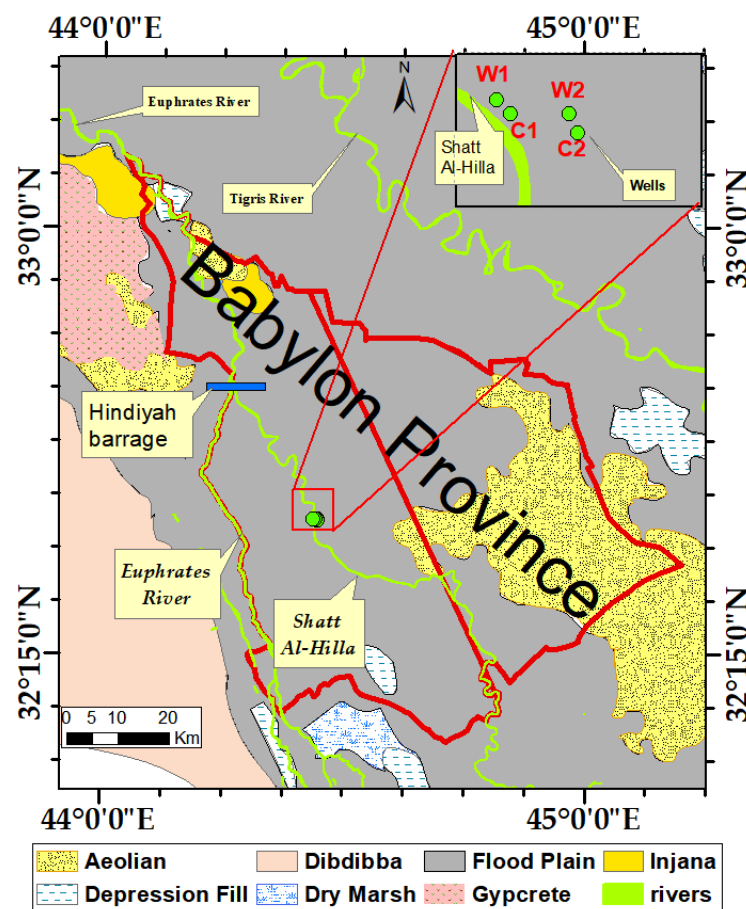


Figure 2. Morphology of the study area [22].

Two predominant morphological units are exposed in the province: flood plain and aeolian landforms. Both of them were developed in the Holocene epoch [21,22].

Quaternary sediments within the region can be ordered from top to bottom as follows: aeolian sediments, flood plain sediments, river terraces, and Mesopotamia fluvial basin sediments [21,22].

Below the Quaternary sediments are the Pre-Quaternary sedimentary rock layers (Pliocene—Early Pleistocene). The Pre-Quaternary sediments can be classified into a number of well-recognized formations, namely the Dibdibba, Mahmudiya, and Bai Hasan formations [22].

2.3. Groundwater Conditions

The aquifer systems in the region are very complex due to the nature of the sediments that built the systems, meaning that the aquifers and aquitards layers cannot be easily

recognized. The layers were built through depositing alternating layers of clay, silty clay, clayey silt, silt, sand, and gravel. The fine sediments consist of aquitards, while the coarse sediments (sand and gravel) form the aquifers. The abrupt lithological conditions increase the complexity of the aquifer systems in the region [23]. In general, the geo-hydrological system in the region can be represented by two aquifer systems: Quaternary and Pre-Quaternary systems. It is assumed that there is a hydraulic continuity between the two aquifer systems (Quaternary and Pre-Quaternary) as well as between the surface water (rivers and lakes) and these two systems [23,24]. The water table in the region is very shallow, being less than 9 m.b.g.s. (metres below the ground surface) [24]. Moreover, some locations have a water table of less than 2 m depth [20] (see Figure 3). The groundwater is rich in chloride and sulphate ions. The total dissolved solids range between 1000 mg/L and 42,200 mg/L [23].

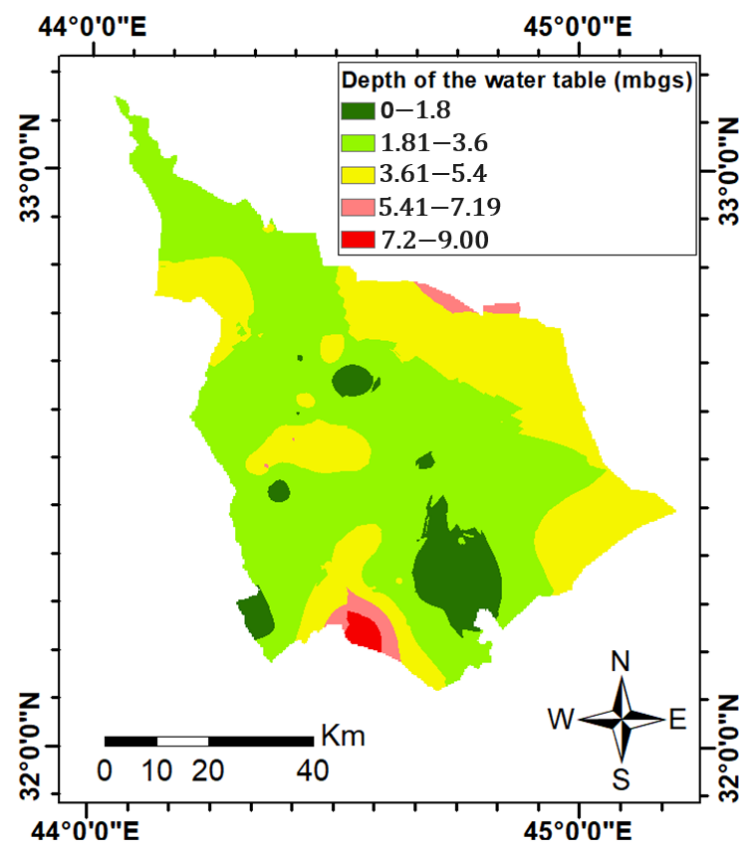


Figure 3. Groundwater depth [20].

2.4. Climate Conditions

According to the Agro-Climatic classification, the study area has an arid climate [25]. The mean annual temperature is about 24 °C. In summer, it can surpass 50 °C. It can also drop below 0 °C in the winter. The average annual precipitation ranges between 100 and 150 mm/year, while the mean annual evaporation is about 3.5 m/year [26].

2.5. Well Locations and Operating Conditions

This study considers a hypothetical ATEs system that is in operation for 20 years in the city of Hilla. Two locations for the system were tested in this study: the first was 75 m from the left bank river, and the other was 300 m from the left bank river. The hypothetical ATEs system consisted of two wells: one for warm storage and the other for cold storage. Each well was 20 m in depth. The distance between the cold well (which is used to store the cold thermal energy) and warm well (which is used to store the warm thermal energy) in each location was about 100 m (Figure 1b). The locations of the four wells in the UTM

units are explained in Table 1. Three pumping rates were considered in each location: 10, 50, and 100 m³/d. We chose to investigate the left side of the river instead of the right side of the river in order to investigate the effect of the river on the system. Since the seepage from the river was superimposed on the regional groundwater flows from the northwest to southeast direction due to the prevailing hydraulic gradient, the losses from the stored energy were maximized due to advection and dispersion losses.

Table 1. Coordinates of the wells in the UTM units.

ATES System	Warm Well			Cold Well			Distance between the System and the River (m)
	Well No.	X(UTM)	Y(UTM)	Well No.	X(UTM)	Y(UTM)	
1	W1	447,247	3,594,779	C1	447,316	3,594,706	75
2	W2	447,614	3,594,706	C2	447,658	3,594,611	300

It was assumed that the temperatures for the cold and warm wells are 12 °C and 36 °C, respectively, while the temperature of the ground was considered to be 24 °C, in accordance with [24].

Climate change significantly affects the seasons within the study area. Summer and winter have become longer than before, while spring and autumn have become shorter [26]. Therefore, for one year of operation, we assumed there needed to be 182 days for heating and 183 days for cooling.

To distinguish between the extraction and the injection wells in the pumping well schedule (within the simulation), a negative sign was assigned to the extraction pumping rates, while a positive sign was assigned to the injection pumping rates.

2.6. Governing Equations

There is a significant similarity between mass and heat transfer. Similar to mass transfer, the heat within porous media transfers in three ways. These ways are conduction (due to thermal gradient), advection (due to groundwater displacement/moving the bulk mass of groundwater), and dispersion (due to the heterogeneity of the medium). Many researchers have noticed the similarity between mass and heat transfer within porous media [27]. As a result, the analogous equation of mass transfer was used to simulate the heat transfer in porous media. The three-dimensional partial differential equation that describes the heat transfer within a homogenous, isotropic media can be described as follows [27–29]:

$$(\rho c)_b \frac{\partial T}{\partial t} = \nabla[(\rho_w c_w \alpha q + \lambda_b) \nabla T] - \rho_w c_w \nabla q T - \rho_w c_w q_s T_s \quad (1)$$

where

$(\rho c)_b \frac{\partial T}{\partial t}$ = Retardation; $\rho_w c_w \alpha q$ = dispersion; $(\lambda_b) \nabla T$ = conduction; $\rho_w c_w \nabla q T$ = advection; $\rho_w c_w q_s T_s$ = mixing.

The subscripts w and b are used to refer to the water and the bulk, ρ is the bulk density (ML⁻³), T is the temperature (°C), c is the heat capacity (L²T⁻²C⁻¹), α is the thermal dispersivity (L), q is the specific discharge (LT⁻¹), λ is the thermal conductivity (ML²T⁻²T⁻¹L⁻¹C⁻¹), ∇T is the temperature gradient, q_s is the source or sink of heat (T⁻¹), and T_s is the temperature of the source (°C).

The term $(\rho c)_b$ can be found from the following equation [29]:

$$(\rho c)_b = \rho_w c_w \theta + \rho_s c_s (1 - \theta) \quad (2)$$

where ρ_s is the density of the solid material of the medium (mass of the solid part divided by the volume of the solid part) (ML⁻³), and c_s is the heat capacity of the solid part of the aquifer (L²T⁻²C⁻¹). Equations (1) and (2) are the fundamental equations that were used in the simulation.

2.7. Model Domain and Meshing

The model domain covers the Babylon Province in central Iraq. A finite difference grid was used in the simulation. To provide good accuracy, the number of columns and rows was specified as 1000 for each. Thus, the cell dimensions are about 114 m in width, and 120 m in length (Figure 4a). Furthermore, to produce a better simulation, the mesh was refined by 10 within the area around the wells (Figure 4b). Thus, the refined cell has a width of 11.4 m and a length of 12.0 m. The vertical direction (stratigraphy) of the region was divided into three layers, with each one being 10 m in thickness (Figure 4c).

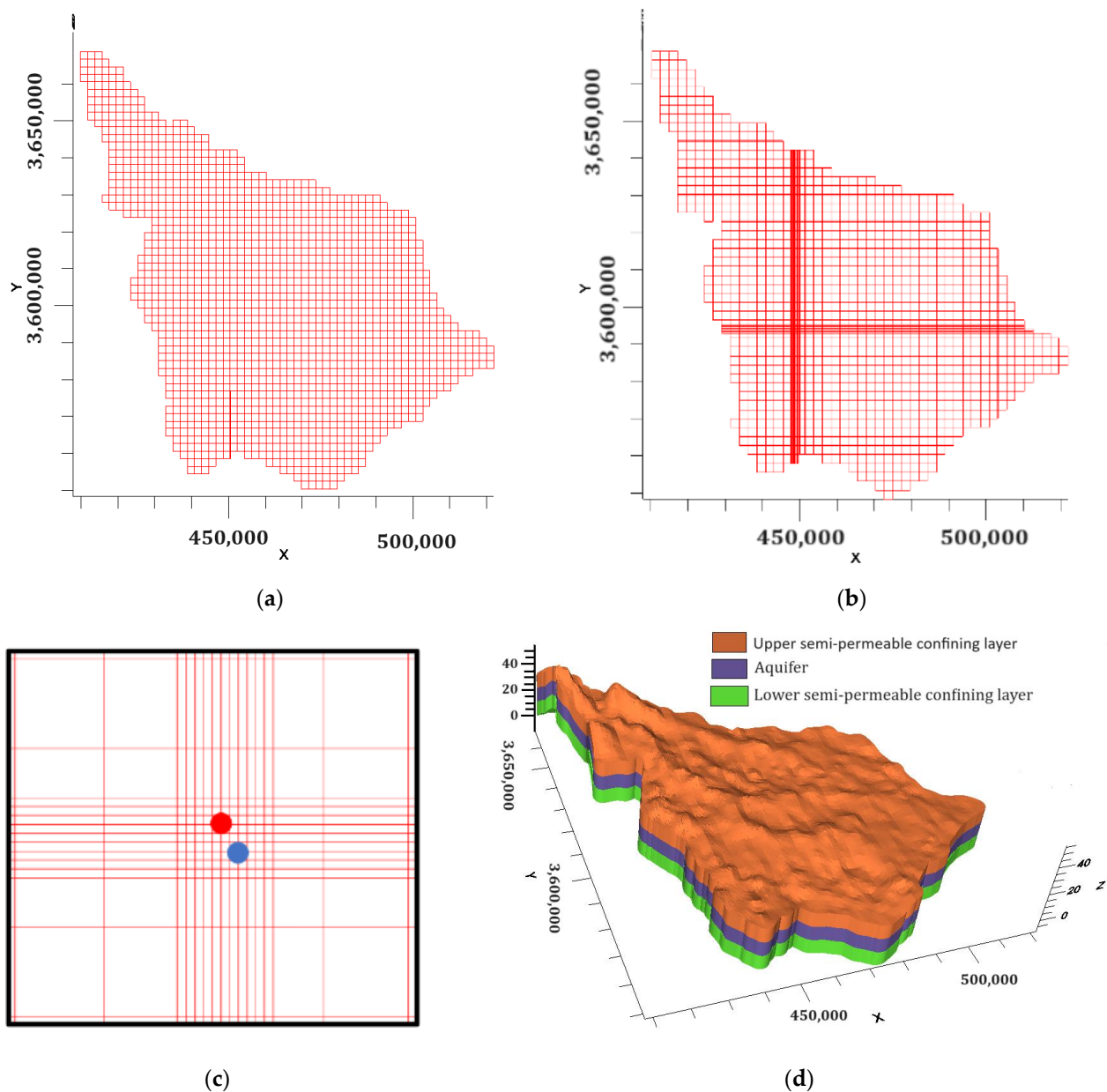


Figure 4. Mesh and layers of the model (a) before refinement and (b) after refinement. (c) Location of the wells; (d) layers of the system.

2.8. Model Parameters

The thermo-hydraulic simulation of the aquifer required inputting the geo-hydrological and the thermal properties of the groundwater, soil, and aquifer. The essential properties for the simulation are listed in Table 2.

Table 2. The geo-hydrological properties of the model [23].

Property	Value	
Aquifer density	1700 kg/m ³	
Water density	1000 kg/m ³	
Compressibility of the water	1 × 10 ⁻⁸ Pa ⁻¹	
Viscosity of the water	0.001 kg/m·d	
Dispersion	10 m	
Total porosity	0.3	
Specific yield	0.2	
Specific storage (Ss)	1 × 10 ⁻⁵ m ⁻¹	
Distribution coefficient (Kd)	2.1 × 10 ⁻⁷ L/mg	
Upper semi-permeable confining layer	Hydraulic conductivity x-direction (Kx)	1 × 10 ⁻⁷ m/s
	Hydraulic conductivity y-direction (Ky)	1 × 10 ⁻⁷ m/s
	Hydraulic conductivity z-direction (Kz)	1 × 10 ⁻⁸ m/s
Aquifer	Hydraulic conductivity x-direction (Kx)	1 × 10 ⁻⁵ m/s
	Hydraulic conductivity y-direction (Ky)	1 × 10 ⁻⁵ m/s
	Hydraulic conductivity z-direction (Kz)	1 × 10 ⁻⁶ m/s
Lower semi-permeable confining layer	Hydraulic conductivity x-direction (Kx)	1 × 10 ⁻⁷ m/s
	Hydraulic conductivity y-direction (Ky)	1 × 10 ⁻⁷ m/s
	Hydraulic conductivity z-direction (Kz)	1 × 10 ⁻⁸ m/s

2.9. Boundary and Initial Conditions

The boundary conditions of the model consist of the surrounding constant heads and the river conditions. Given the geography of the study area, it can be considered as a triangle (Figure 3a). Consequently, the constant heads' boundary conditions can be represented by three sides: the eastern, western, and southern sides. To assign the constant head values along these sides, a map of groundwater elevation above sea level was required (Figure 5b). This map was found by subtracting the value for groundwater elevation below the ground surface from the ground surface elevation. This process can be performed by using the raster calculator tool within ArcMap/GIS 10.8 software. The resultant map of the groundwater elevation above sea level is presented in Figure 5b. The elevation of the groundwater decreases in the southeast direction. This explains why the groundwater in this region flows from the northwest towards the southeast. Based on Figure 5b, in our modelling stage, it was assumed that the constant heads of the three sides change linearly. The values of the constant heads at the three corners (A, B, and C in Figure 5a) of the region are 39.99, 17.2, and 21.7 m, respectively.

There are three main river systems in the region. These are the Euphrates River upstream of the Hindiyah Barrage, the Euphrates River downstream of the Hindiyah Barrage, and Shatt Al-Hilla (Figure 5c). All these rivers flow from the northwest towards the southeast, matching the slope of the ground surface noted above. The conditions of these rivers are summarized in Table 3.

2.10. Simulation

The simulation was initiated by preparing the essential maps using ArcMap/GIS software. These maps include a boundary of the region as a polygon shape file, ground surface as a raster file, the upper and lower beds of the layers that represent the stratigraphy of the region as a raster file, constant head boundary conditions (east, west, and south) as a line shape file, and the courses of the rivers flowing within the study area as a line shape file. ArcMap was also used to identify the UTM coordinates of the cold and warm wells.

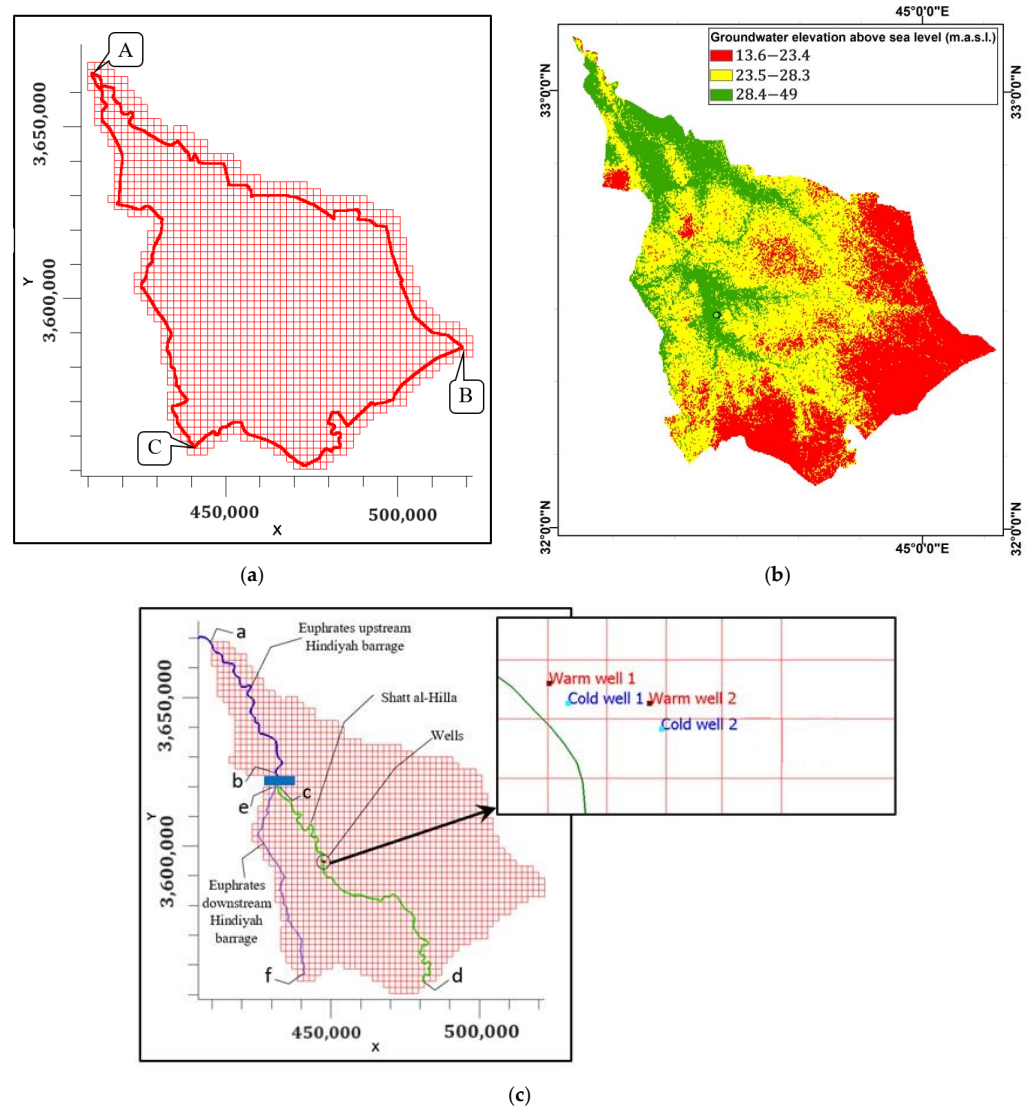


Figure 5. Boundary conditions of the study area: (a) constant head boundaries; (b) groundwater elevation within the study area; (c) main rivers of the study area.

Table 3. Conditions of the rivers within the study area ¹.

Conditions	Euphrates Upstream of Hindiyah Barrage		Euphrates Downstream of Hindiyah Barrage		Shatt Al-Hilla	
	a	b	c	d	e	f
Stage (m) ^{2,3}	36.1	31.7	26.85	24.88	29.6	27.6
Bottom (m) ^{2,4}	33.1	27.3	23.3	19.6	26.4	24.4
Riverbed thickness (m) ²	0.5	0.5	0.5	0.5	0.5	0.5
River width (m) ⁴	240	140	120	100	73	60
River conductivity (m/s) ⁵	1×10^{-6}	1×10^{-6}	1×10^{-6}	1×10^{-6}	1×10^{-4}	1×10^{-4}
Temperature (°C) ⁶	24	24	24	24	24	24

Notes: ¹ For the points (a, b, c, d, e, and f), see Figure 5c. ² Based on [30]. ³ Based on [31]. ⁴ Based on [32]. ⁵ Based on [33]. ⁶ Based on [24].

3. Results and Discussion

3.1. System at 75 m from the River

The orange dots in Figures 6–8 represent the warm and cold wells, while the blue dots represent the Shatt Al-Hilla River. The blue dots appear in the surface layer only since the

depth of the river (3.2 m) does not penetrate the surface layer (10 m thickness). In the same way, the wells (orange dots) do not appear in the lower layer since the well depth (20 m) does not reach the lower layer (20–30 m depth).

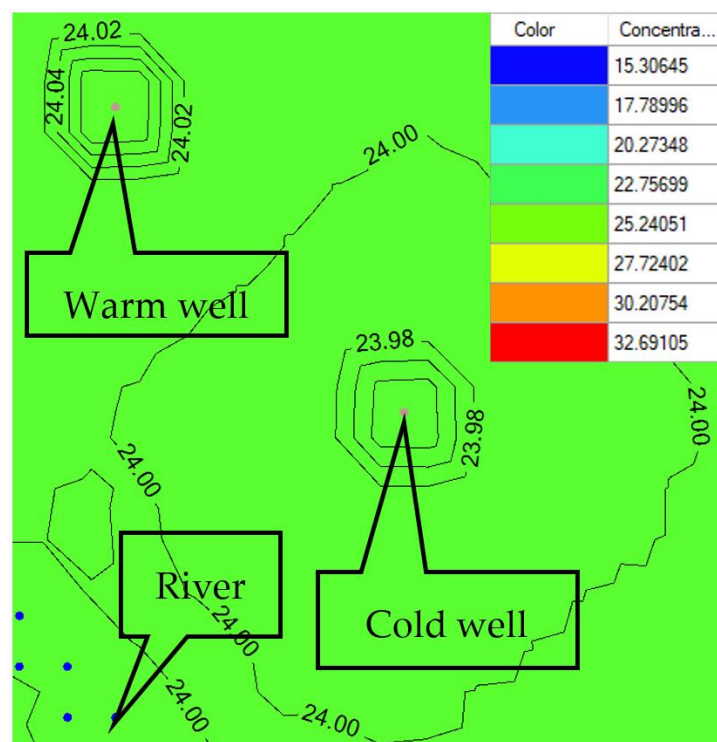
The system in this location was simulated under three pumping rates: 10 m³/d, 50 m³/d, and 100 m³/d. The same pumping rates were also used for the other location (300 m from the river).

For a 10 m³/d pumping rate, the thermal waves for the three layers (upper “surface”, middle “storage”, and lower) after one year and twenty years of operation are shown in Figure 6a–f. Figure 6a,c,e show the three layers of the system after one year of operation, while Figure 6b,d,f show the layers after twenty years.

Considering the system after one year for the surface layer, the average temperatures within the cells (11.4 m × 12.04 m) of the warm and cold wells are 24.29 °C and 23.82 °C, respectively, Figure 6a. The thermal fronts of 24.02 °C and 23.98 °C along the axis between the wells (critical path) are both about 25.15 m from the warm and cold wells, respectively. The distance between the two waves is about 49.74 m. This produces a thermal gradient of about 8.04 × 10⁻⁴ °C/m. There is no discernible interference between the two waves since they do not affect each other (Figure 4a).

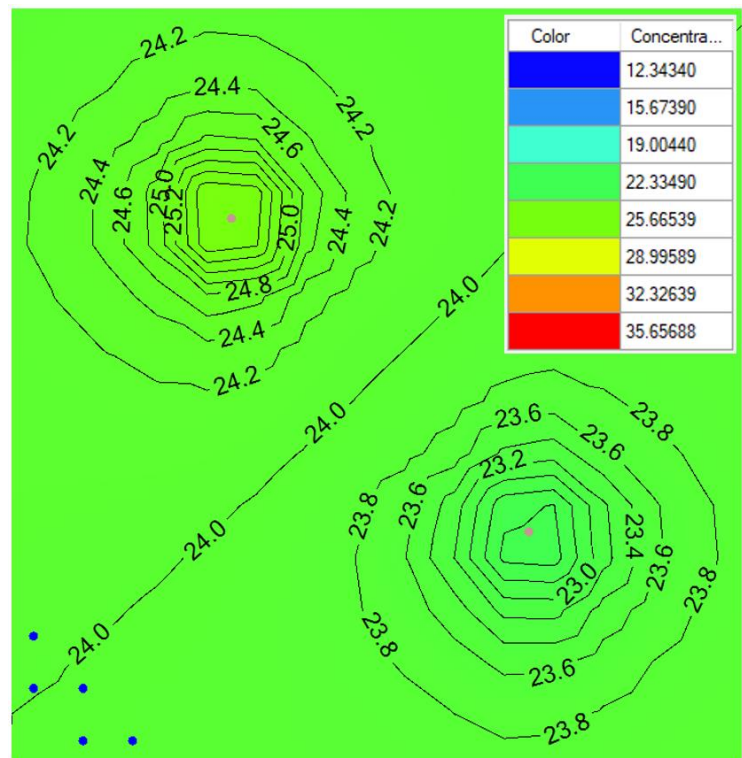
After twenty years of operation at 10 m³/d pumping rate (Figure 6b), the surface layer demonstrates an increase in the stored energy. The cold and warm thermal fronts are 23.8 °C and 24.2 °C, closer to each other than the first-year operation.

Considering the middle layer (Figure 6c,d), for a 10 m³/d pumping rate, the stored energy is much noticeable in this layer. The reasons behind this are twofold: the screens of the injection wells are within this layer, and the fact that this layer has high hydraulic conductivity compared to the upper (Figure 6a,b) and lower (Figure 6e,f) layers. After one year of operation (Figure 6c), the stored energy increased to the point where the thermal fronts were 25 °C and 23 °C. These fronts became closer to each other after twenty years of operation. This increased the thermal losses due to interference of the thermal front.

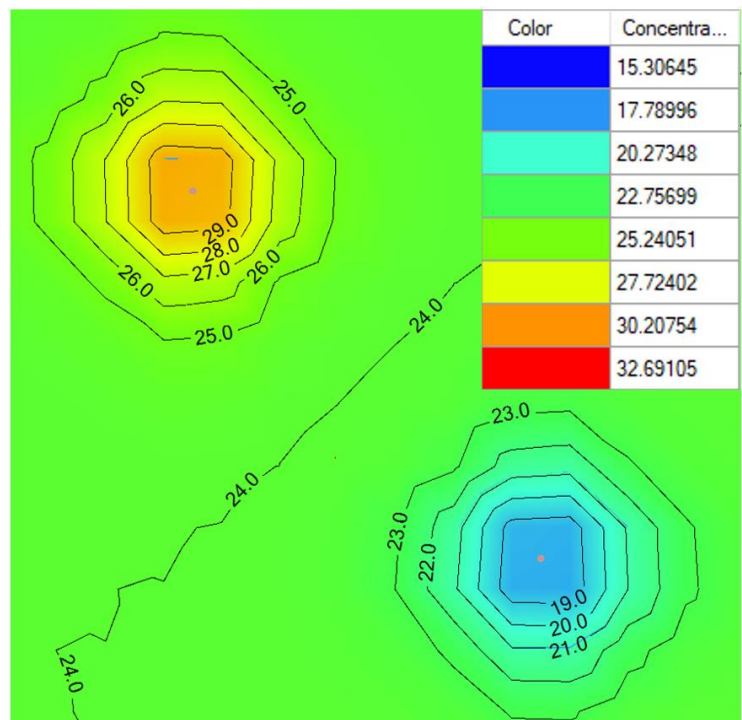


(a)

Figure 6. Cont.

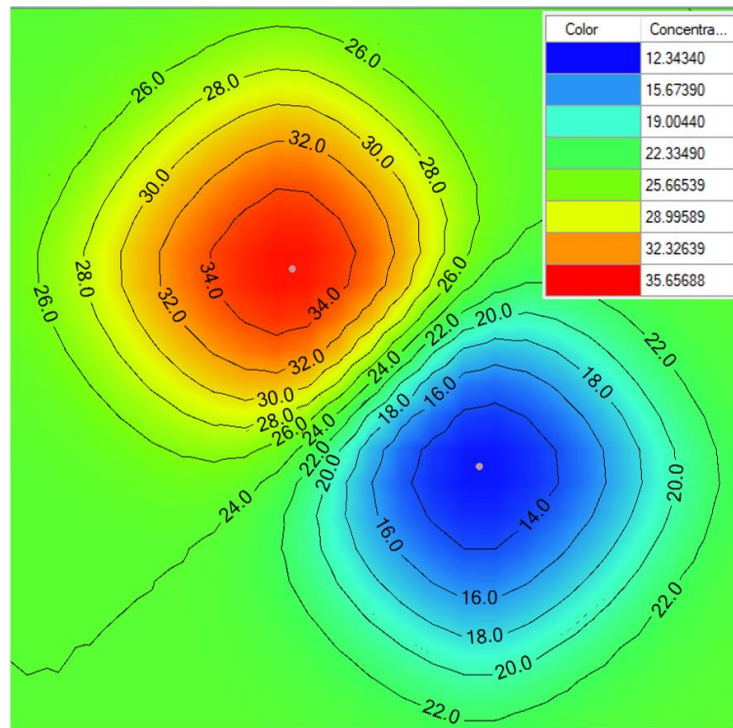


(b)

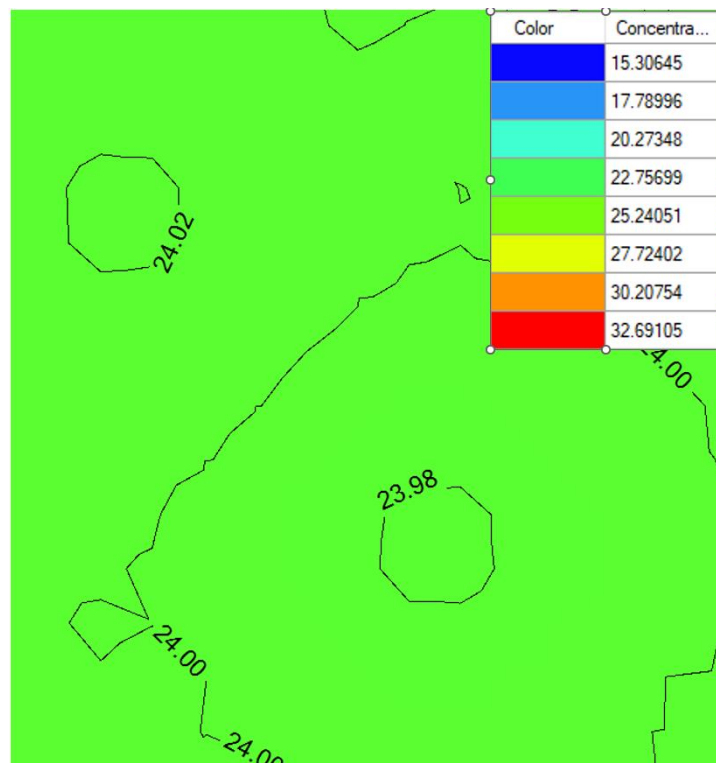


(c)

Figure 6. Cont.

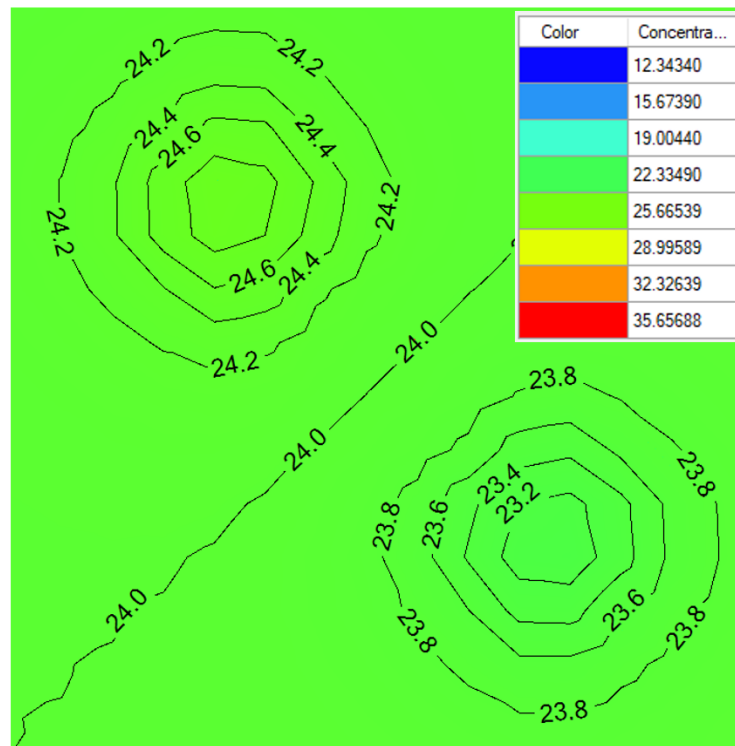


(d)



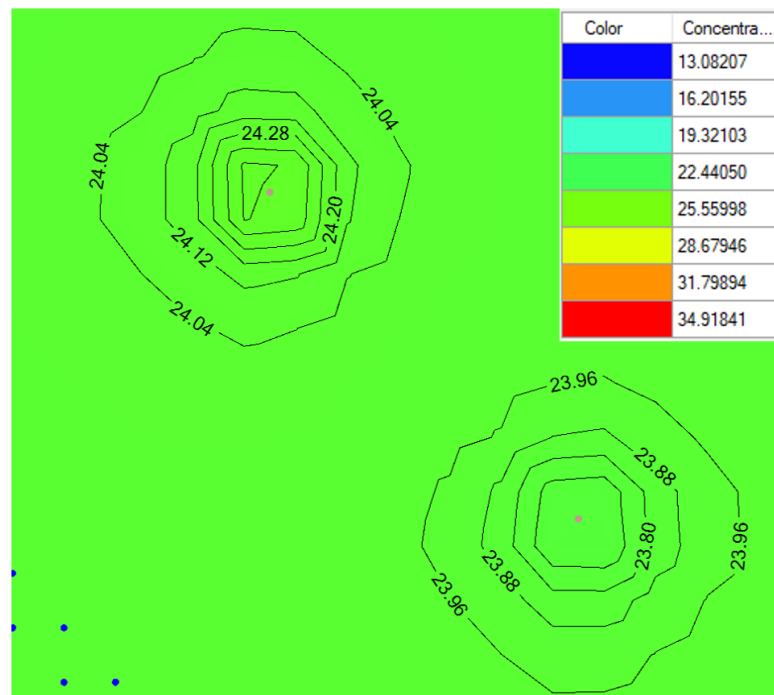
(e)

Figure 6. Cont.



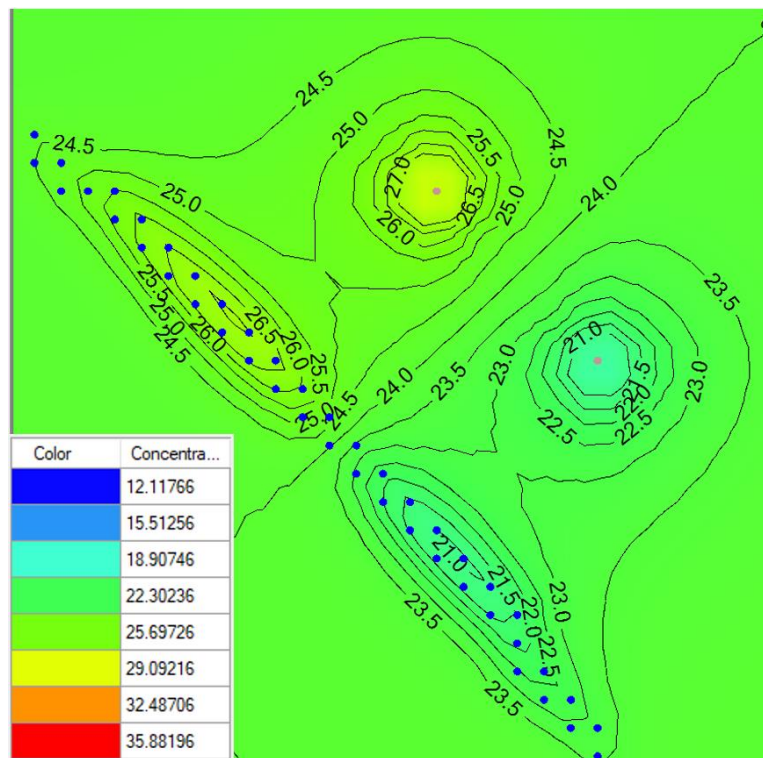
(f)

Figure 6. Simulation of the ATEs system at 75 m from the river and $q = 10 \text{ m}^3/\text{d}$ after 1 year and 20 years of operation: (a) first layer after 1 year; (b) first layer after 20 years; (c) second layer after 1 year; (d) second layer after 20 years of operation; (e) third layer after 1 year; (f) third layer after 20 years.

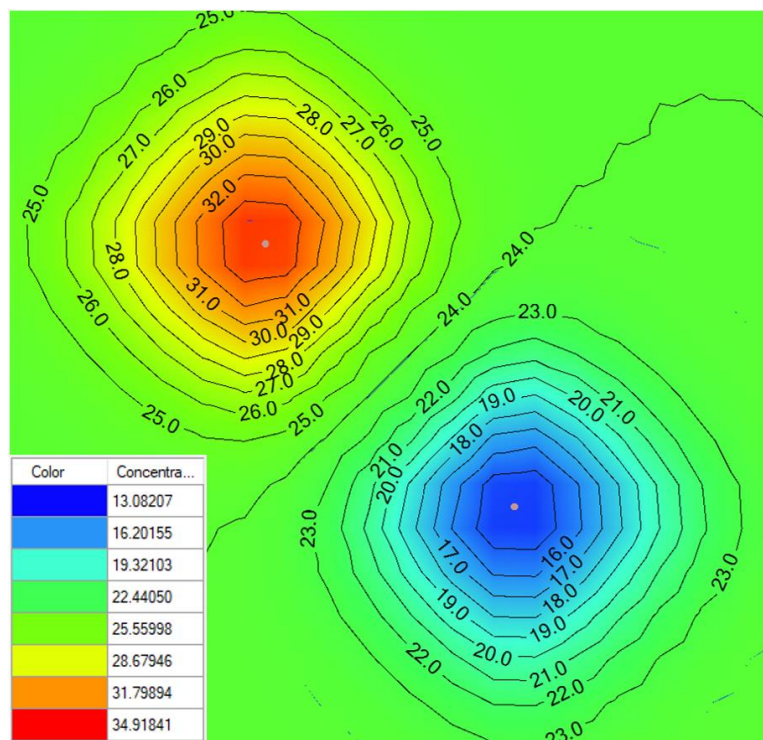


(a)

Figure 7. Cont.

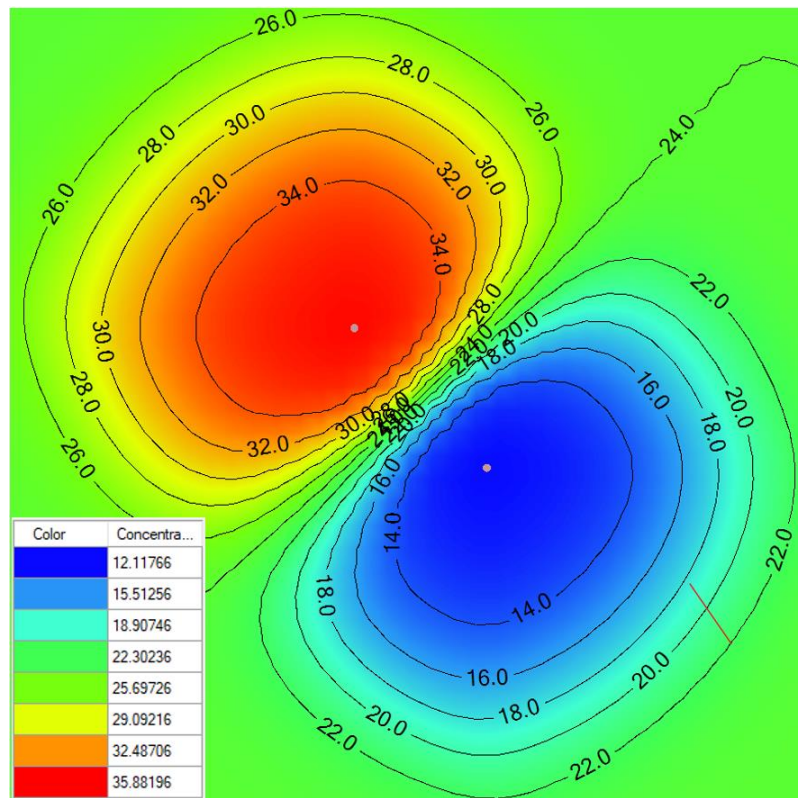


(b)

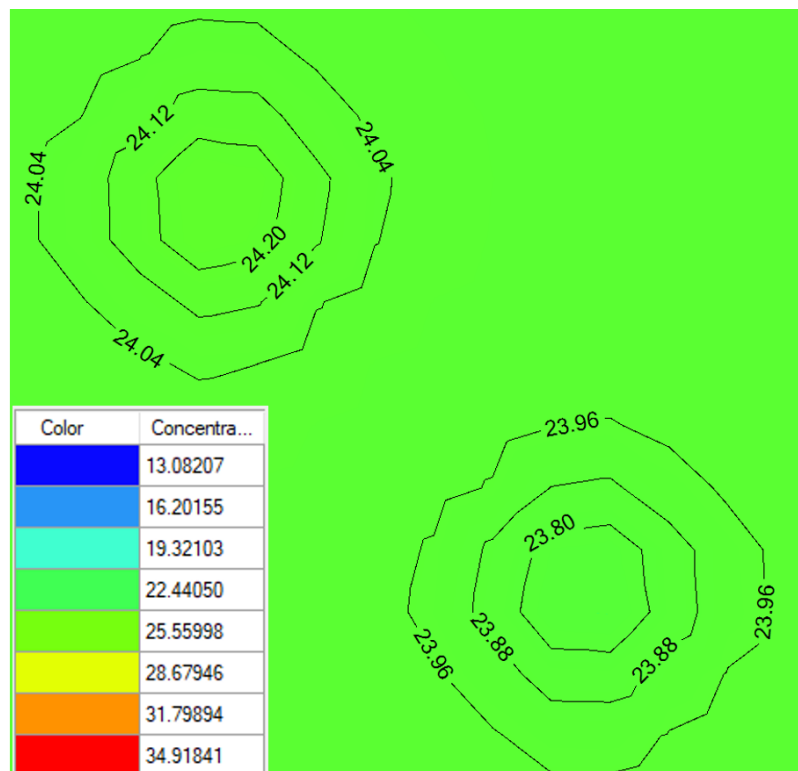


(c)

Figure 7. Cont.

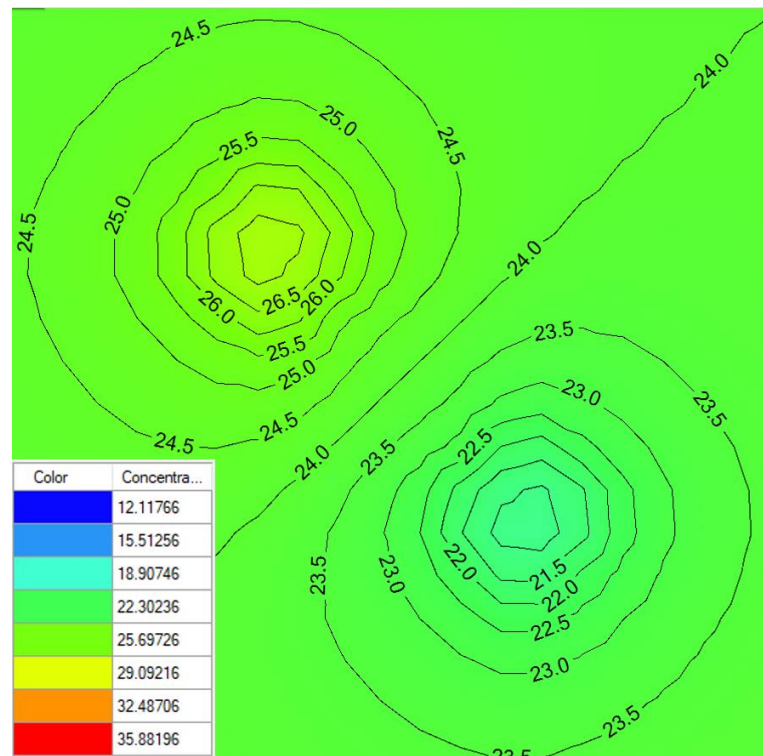


(d)



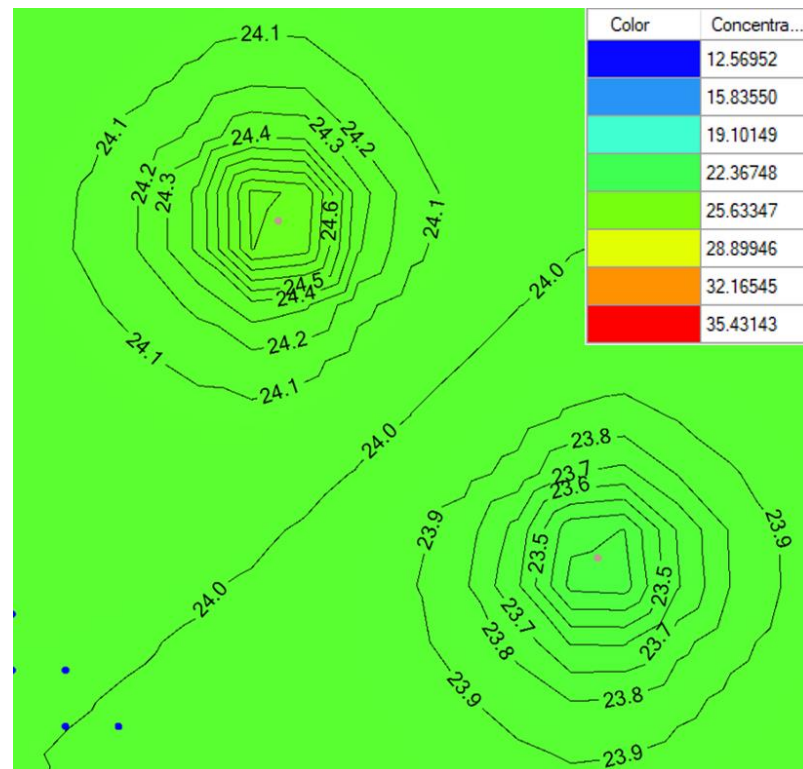
(e)

Figure 7. Cont.



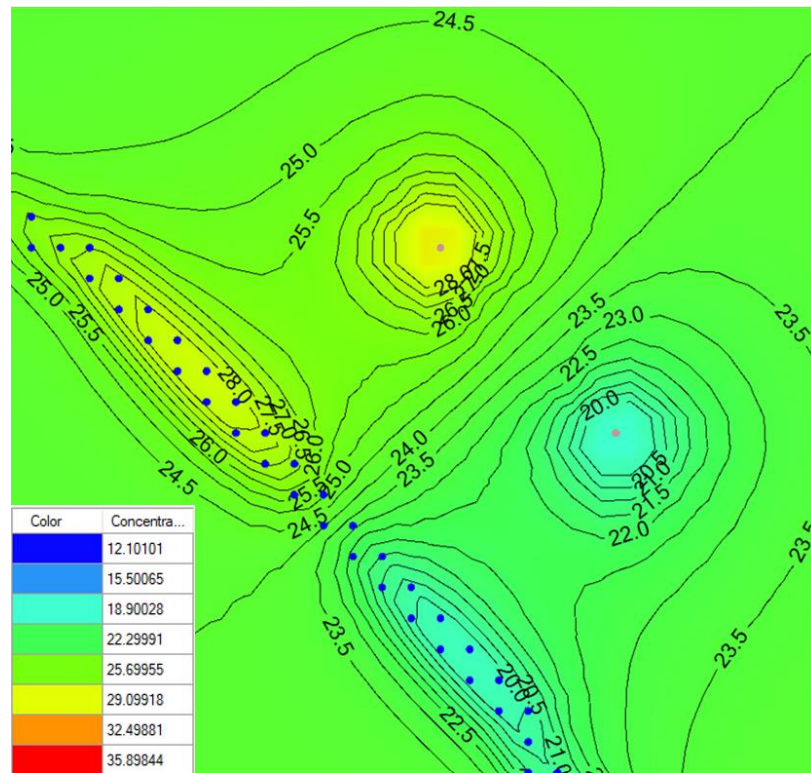
(f)

Figure 7. Simulation of the ATEs system at 75 m from the river and $q = 50 \text{ m}^3/\text{d}$ after 1 year and 20 years of operation: (a) first layer after 1 year; (b) first layer after 20 years; (c) second layer after 1 year; (d) second layer after 20 years of operation; (e) third layer after 1 year; (f) third layer after 20 years.

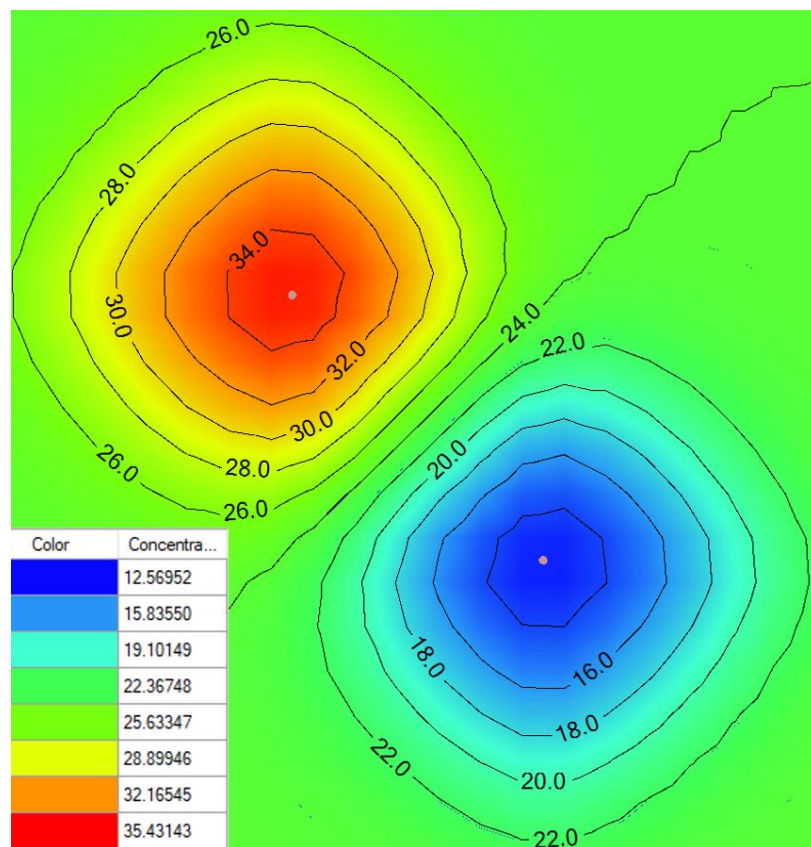


(a)

Figure 8. Cont.

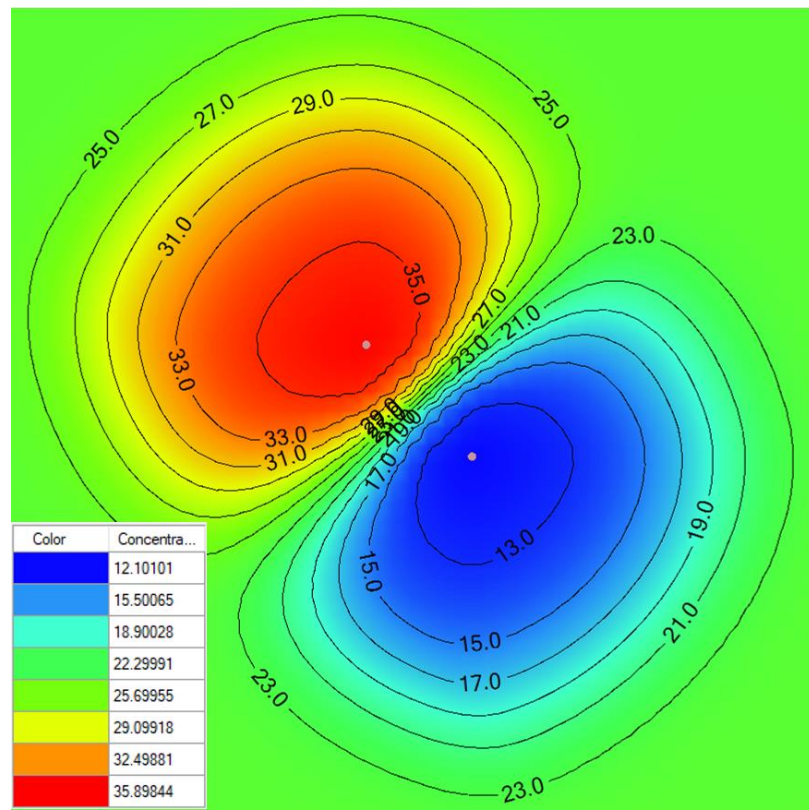


(b)

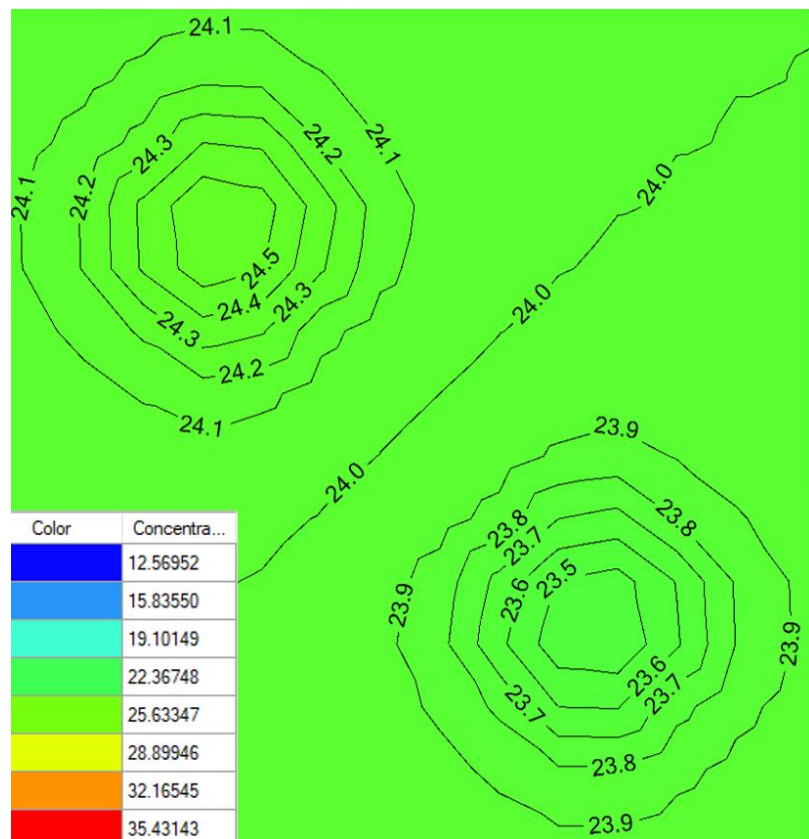


(c)

Figure 8. Cont.

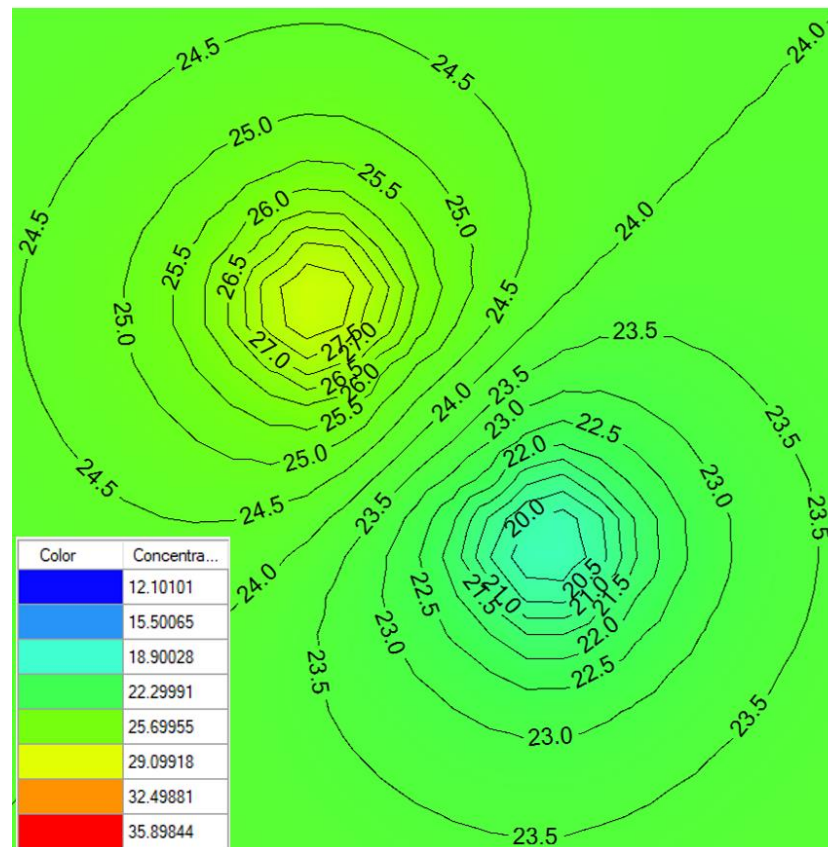


(d)



(e)

Figure 8. Cont.



(f)

Figure 8. Simulation of the ATES system at 75 m from the river and $q = 100 \text{ m}^3/\text{d}$ after 1 year and 20 years of operation: (a) first layer after 1 year; (b) first layer after 20 years; (c) second layer after 1 year; (d) second layer after 20 years of operation; (e) third layer after 1 year; (f) third layer after 20 years.

Considering the lower layer (Figure 6e,f) at a $10 \text{ m}^3/\text{d}$ pumping rate, the stored energy is less than the stored energy in the storing layer (middle layer) since the screens of the wells are not in this layer. The second reason for this is the low hydraulic conductivity of this layer, which produces low heat transfer, according to Equation (1).

It is logical that all thermal changes increase by increasing the pumping rates (Figures 7 and 8). Considering the system after one year of operation under a $50 \text{ m}^3/\text{d}$ pumping rate, the temperature within the well cells are $24.08 \text{ }^\circ\text{C}$, $29 \text{ }^\circ\text{C}$, and $24.02 \text{ }^\circ\text{C}$ for the warm wells and $23.94 \text{ }^\circ\text{C}$, $19 \text{ }^\circ\text{C}$, and $23.98 \text{ }^\circ\text{C}$ for the cold wells for the upper, middle, and lower layers, respectively (Figure 7a,c,e). These temperature changes increased after twenty years of operation to $25.6 \text{ }^\circ\text{C}$, $34 \text{ }^\circ\text{C}$, and $24.8 \text{ }^\circ\text{C}$ for the warm wells and $28.6 \text{ }^\circ\text{C}$, $14 \text{ }^\circ\text{C}$, and $23.2 \text{ }^\circ\text{C}$ for the cold wells for the upper, middle, and lower layers, respectively (Figure 7b,d,f).

It is worth mentioning that increasing the pumping rate causes the thermal wave fronts in all directions, including the direction within the river, to increase (Figure 7b). This leads to the stored energy leaking into the river. The energy leaks derive from both the cold and warm wells. This decreases the efficiency of the system. The effect of the river is limited within the upper layer only since the depth of river is within this layer.

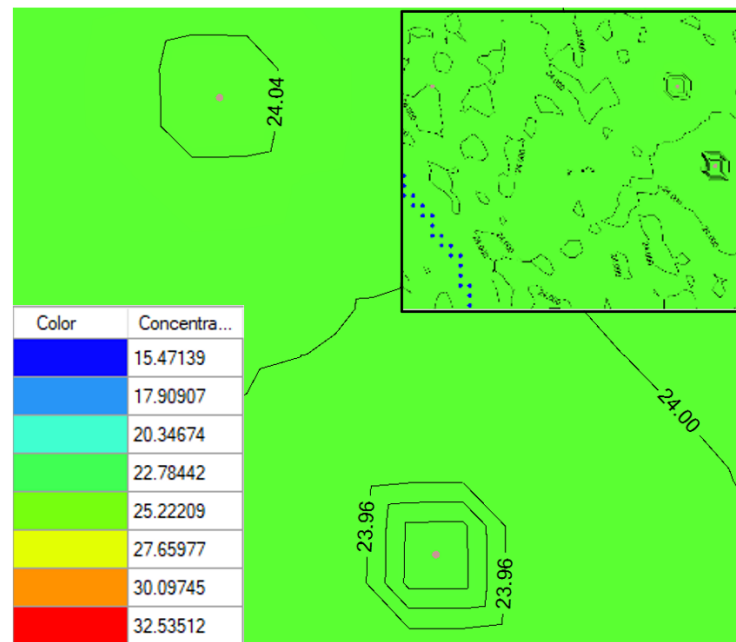
After twenty years of operation (Figure 7b), the thermal wave fronts spread so that two centres appear in the river. Each one corresponds to a well. The temperature in the cold and warm centres are the same temperature in the cold and warm wells, respectively.

Considering the system at a $100 \text{ m}^3/\text{d}$ pumping rate (Figure 8a–f), the thermal changes increase more than the ones corresponding to the $10 \text{ m}^3/\text{d}$ and $50 \text{ m}^3/\text{d}$ pumping rates. These increases produce more leaks into the river (Figure 6b). The temperature of the cold

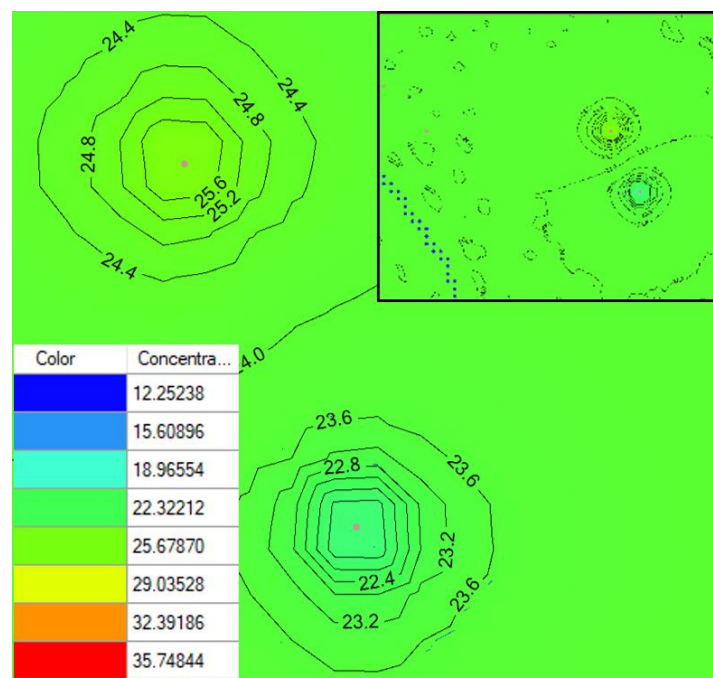
and the warm centres in the river are 20 °C and 28 °C. The thermal waves can be configured very well by increasing the pumping rates (Figures 7b and 8b).

3.2. System at 300 m from the River

For the 10 m³/d pumping rate, thermal waves for the three layers (upper, middle, and lower) after one and twenty years of operation are shown in Figure 9a–f. Figure 9a,c,e show the three layers of the system after one year of operation, while Figure 9b,d,f show the layers after twenty years of operation. The results for the 50 and 100 m³/d rates of flow are presented in Figures 10 and 11, respectively.

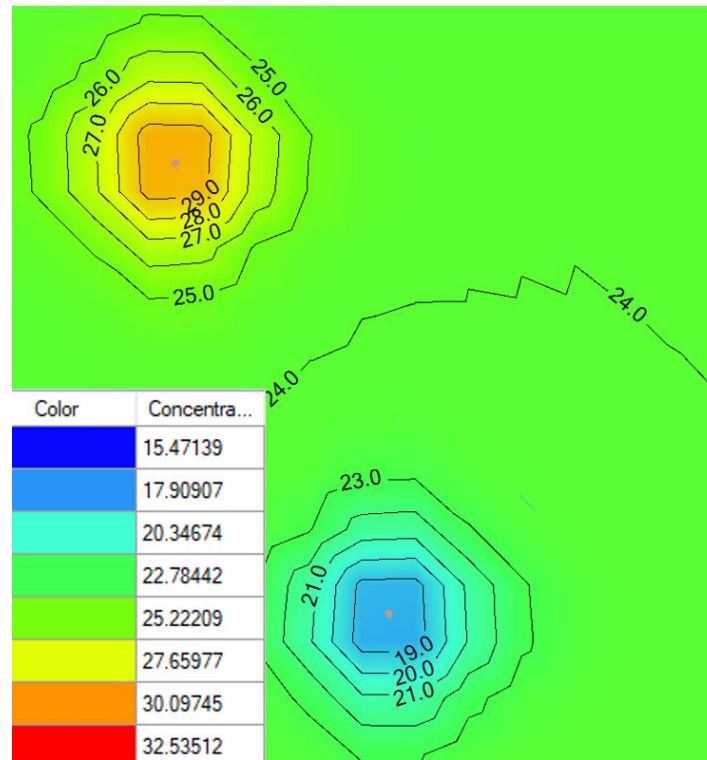


(a)

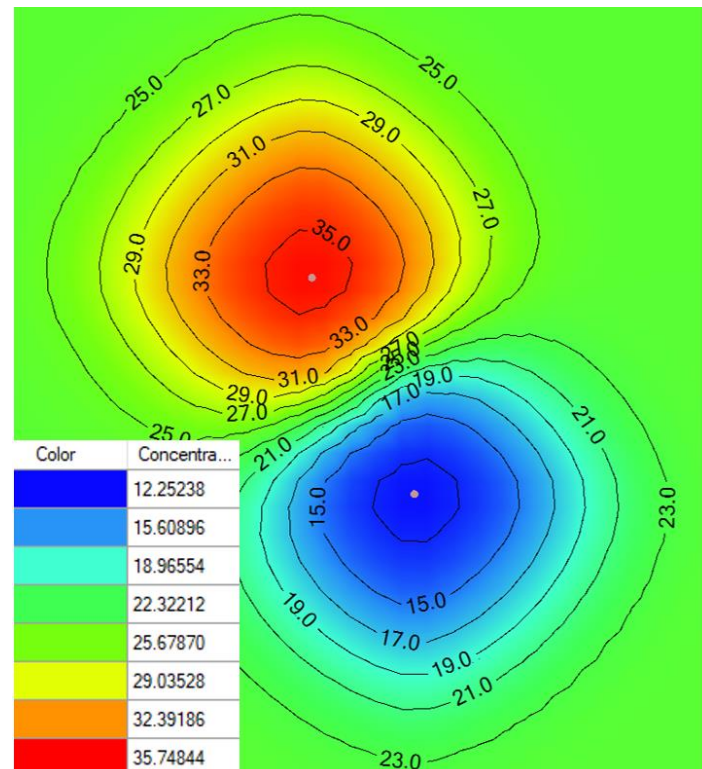


(b)

Figure 9. Cont.

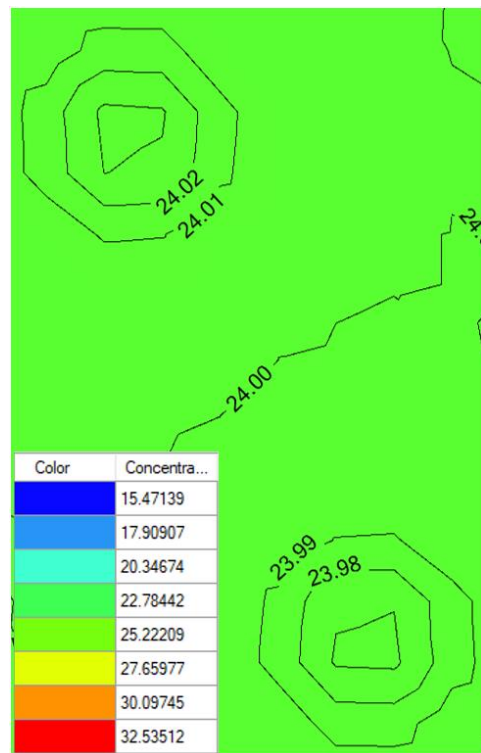


(c)

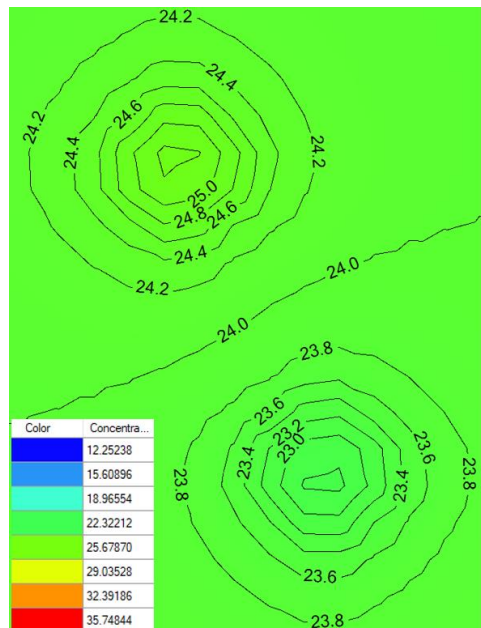


(d)

Figure 9. Cont.

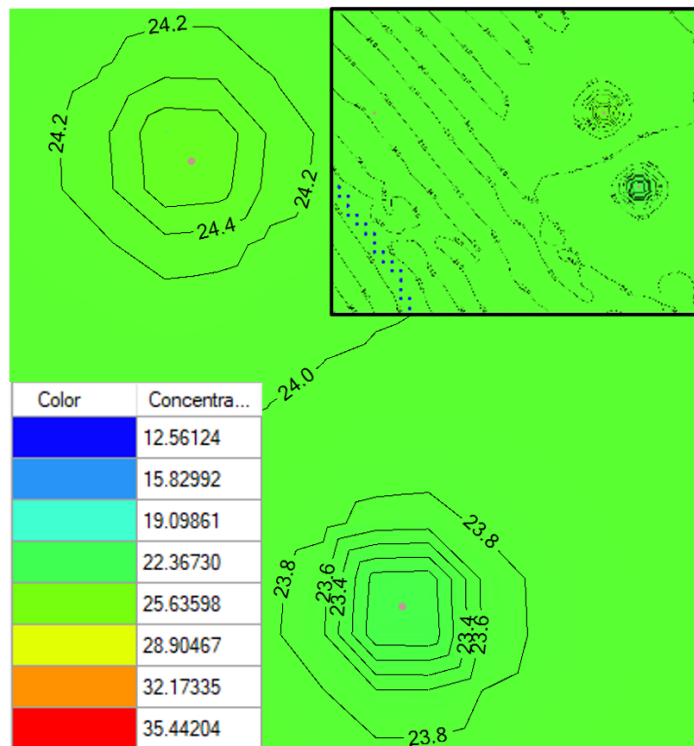


(e)

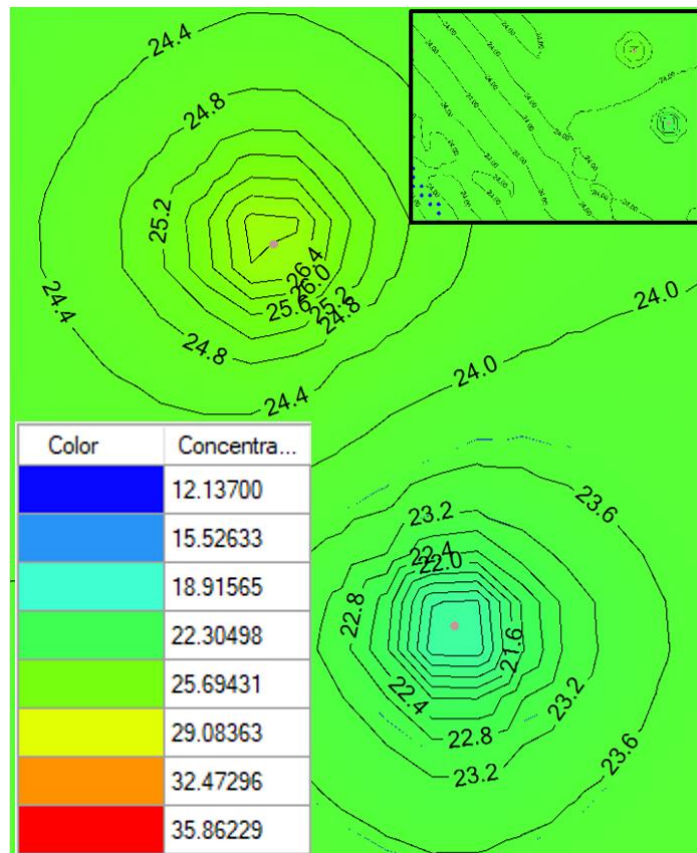


(f)

Figure 9. Simulation of the ATEs system when 300 m away from the river and $q = 10 \text{ m}^3/\text{d}$ after one year and twenty years of operation: (a) first layer after one year; (b) first layer after twenty years; (c) second layer after one year; (d) second layer after twenty years of operation; (e) third layer after one year; (f) third layer after twenty years.

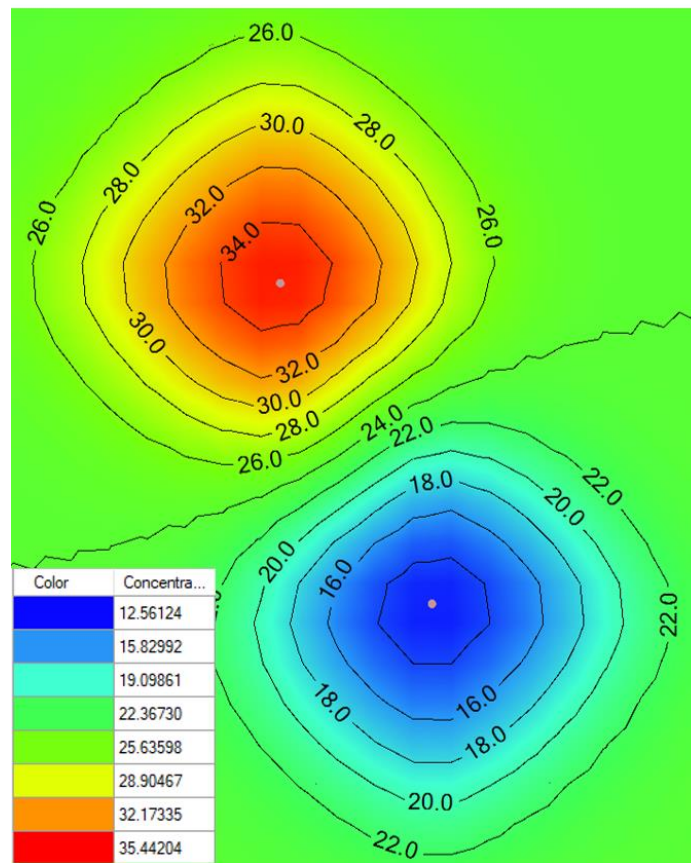


(a)

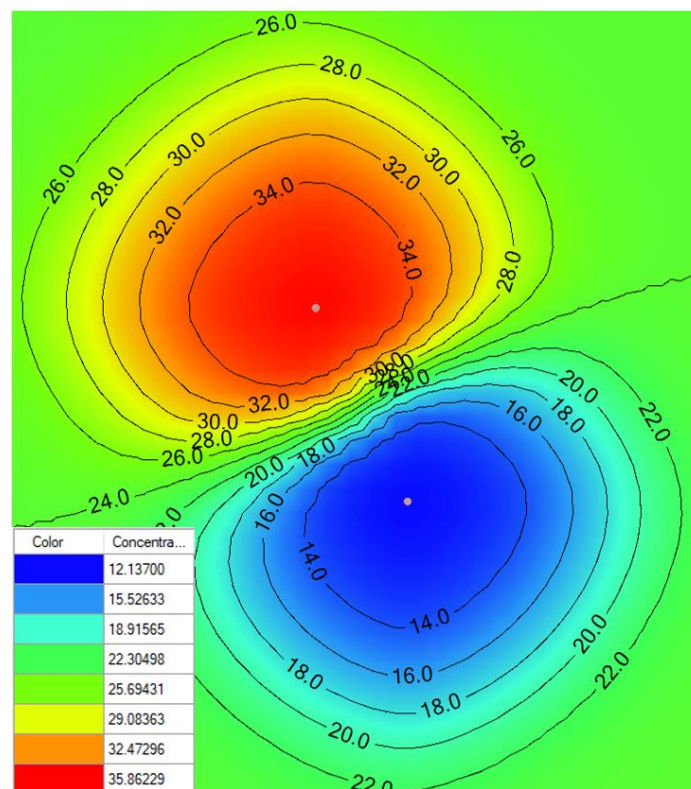


(b)

Figure 10. Cont.

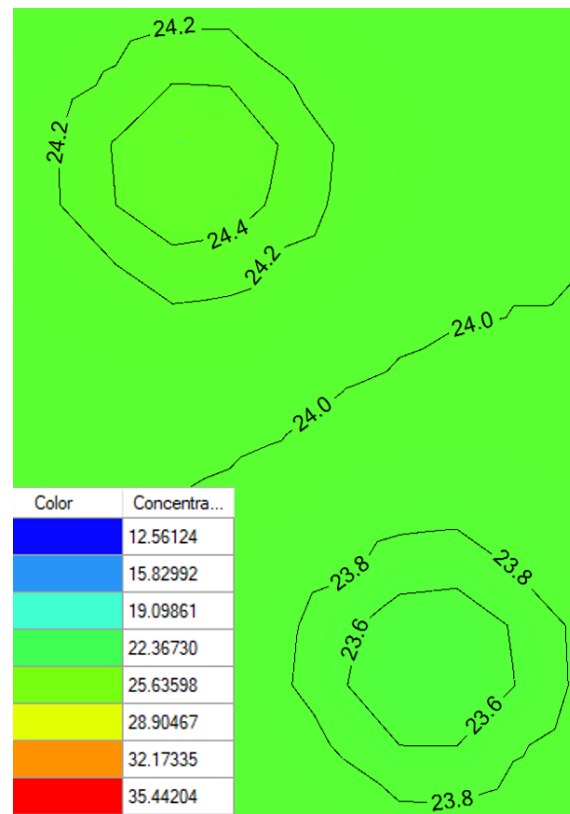


(c)

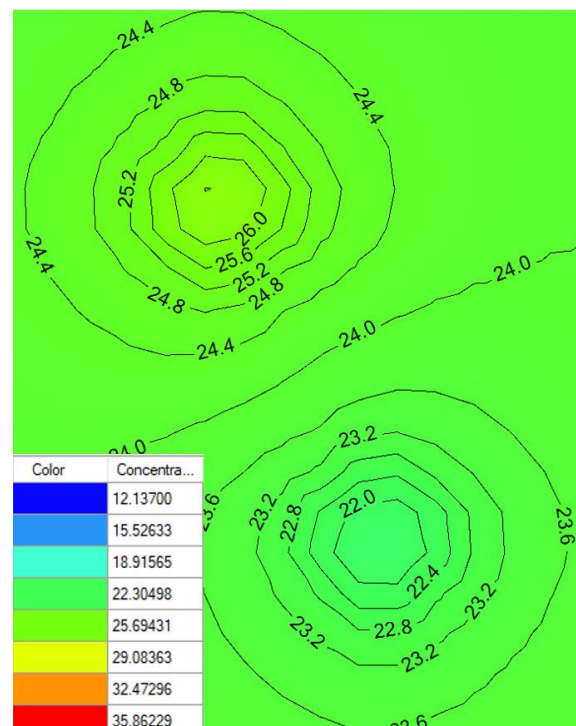


(d)

Figure 10. Cont.

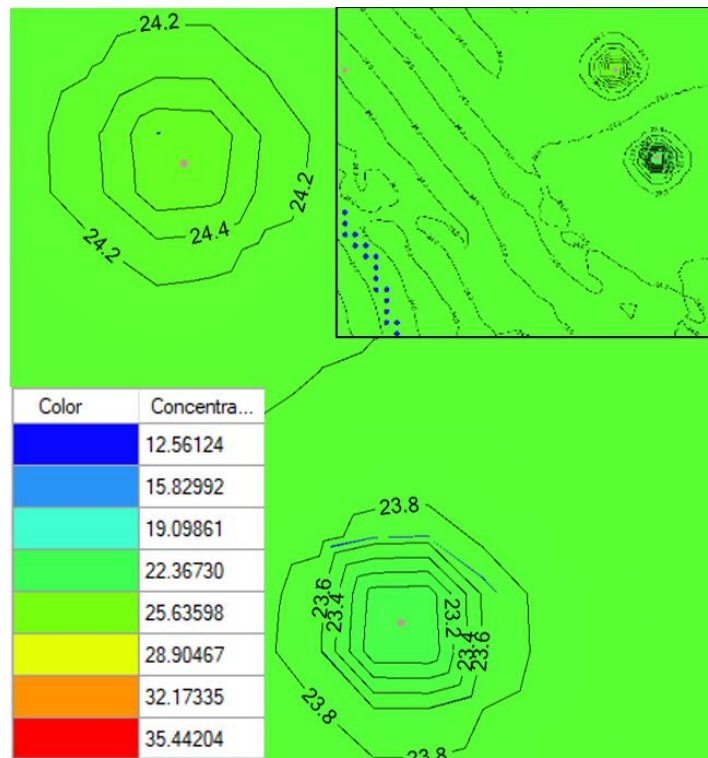


(e)

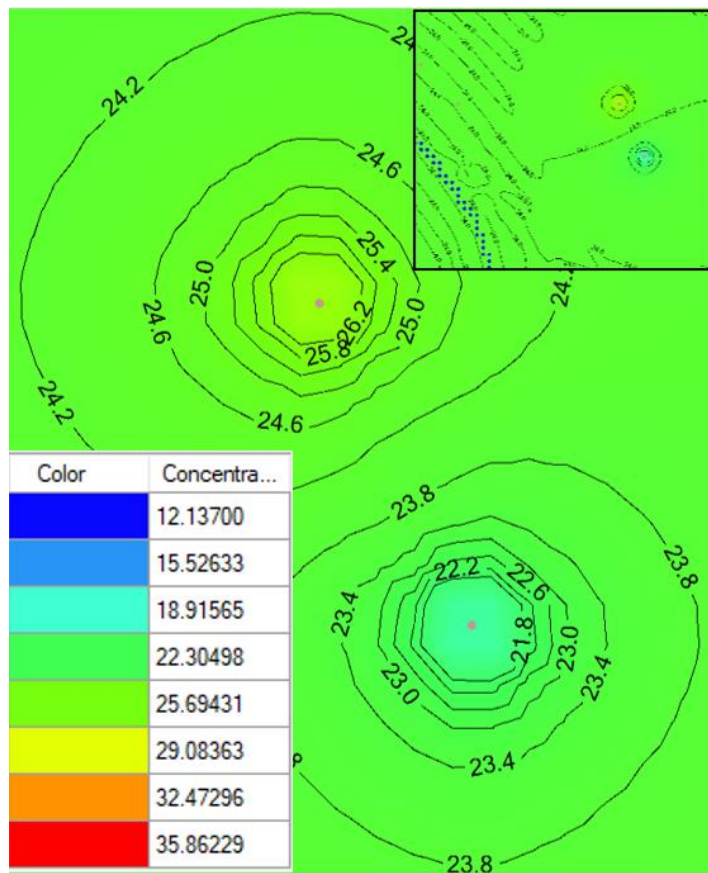


(f)

Figure 10. Simulation of the ATEs system at 300 m away from the river and $q = 50 \text{ m}^3/\text{d}$ after one year and twenty years of operation: (a) first layer after one year; (b) first layer after twenty years; (c) second layer after one year; (d) second layer after twenty years of operation; (e) third layer after one year; (f) third layer after twenty years.

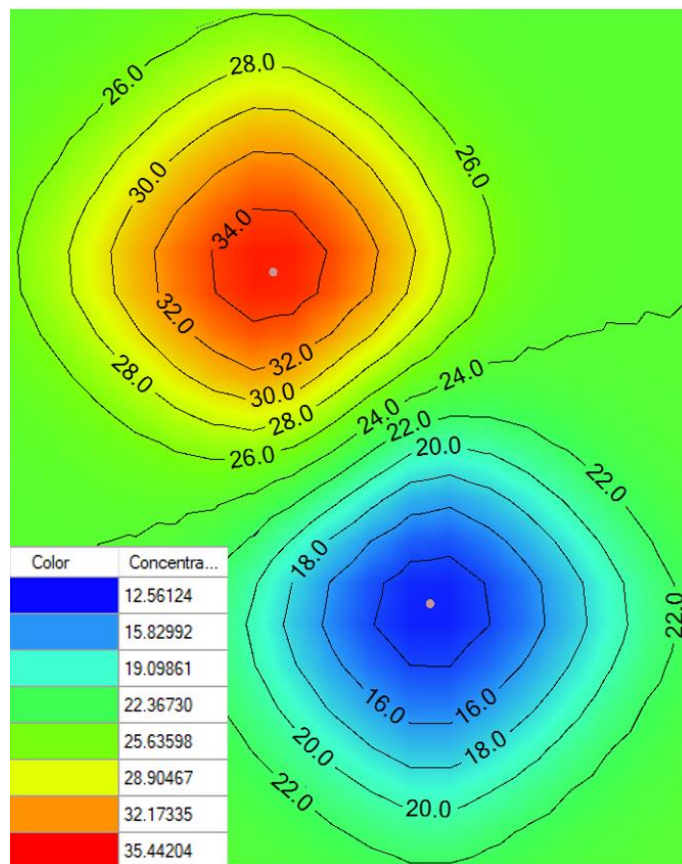


(a)

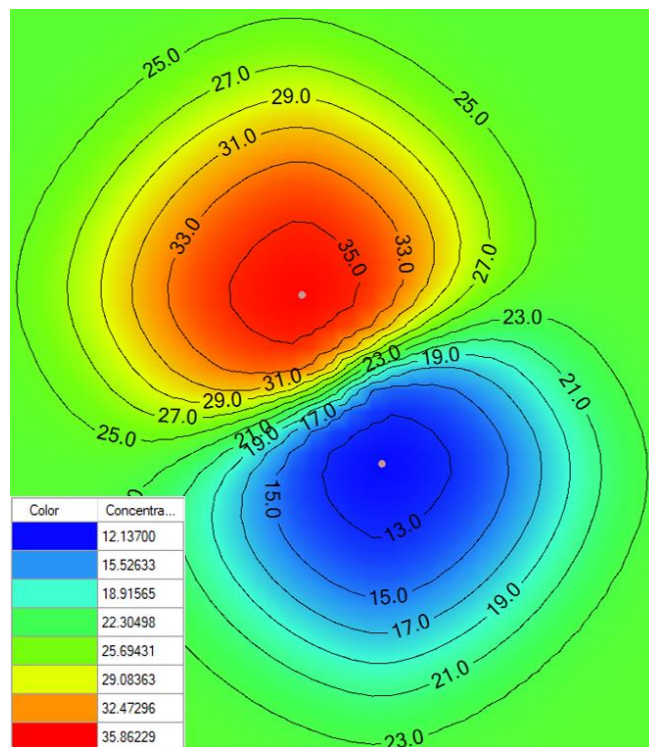


(b)

Figure 11. Cont.

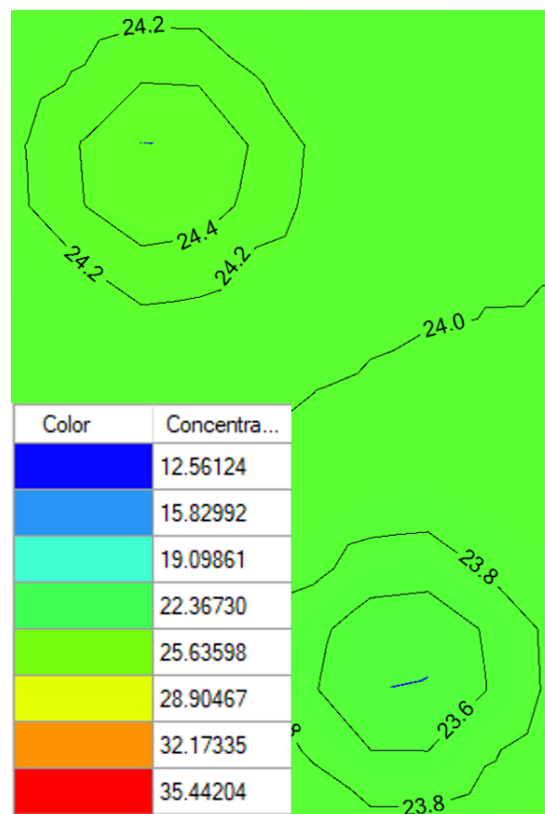


(c)

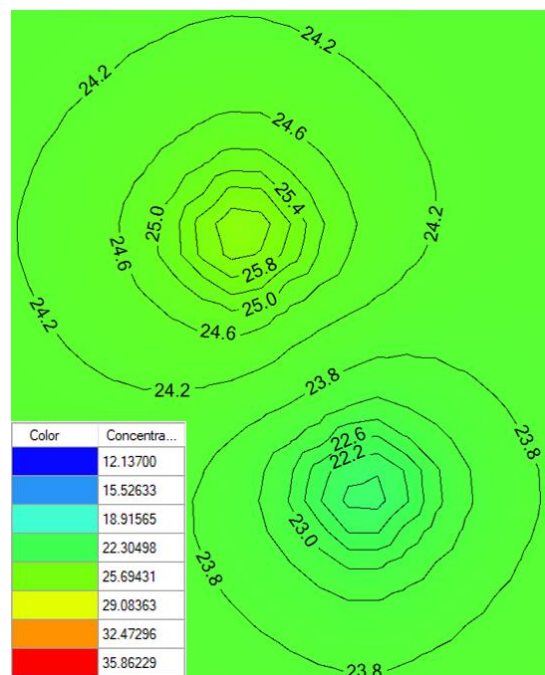


(d)

Figure 11. Cont.



(e)



(f)

Figure 11. Simulation of the ATEs system at 300 m away from the river and $q = 100 \text{ m}^3/\text{d}$ after one year and twenty years of operation: (a) first layer after one year; (b) first layer after twenty years; (c) second layer after one year; (d) second layer after twenty years of operation; (e) third layer after one year; (f) third layer after twenty years.

It is worth mentioning that, when the system is 300 m away from the river and under specific pumping rates (Figures 9–11), the thermal waves develop in the same way as they did when the system was 75 m away from the river (Figures 6–8), except for one main difference: the effect of the river. In the case where the system is 300 m away from the river, there are no losses from the system to the river since there is no interface between the river and the wells. This increases the efficiency of the system compared to the case where the system is 75 m away from the river.

3.3. Seepage Velocity Direction Map

Visual MODFLOW (VMOD) Flex (version 6.1) software was used to produce a seepage velocity direction map. A map depicting for the direction of the seepage velocity within the study area is shown in Figure 12. The groundwater flows from the northwest direction to the southeast direction.

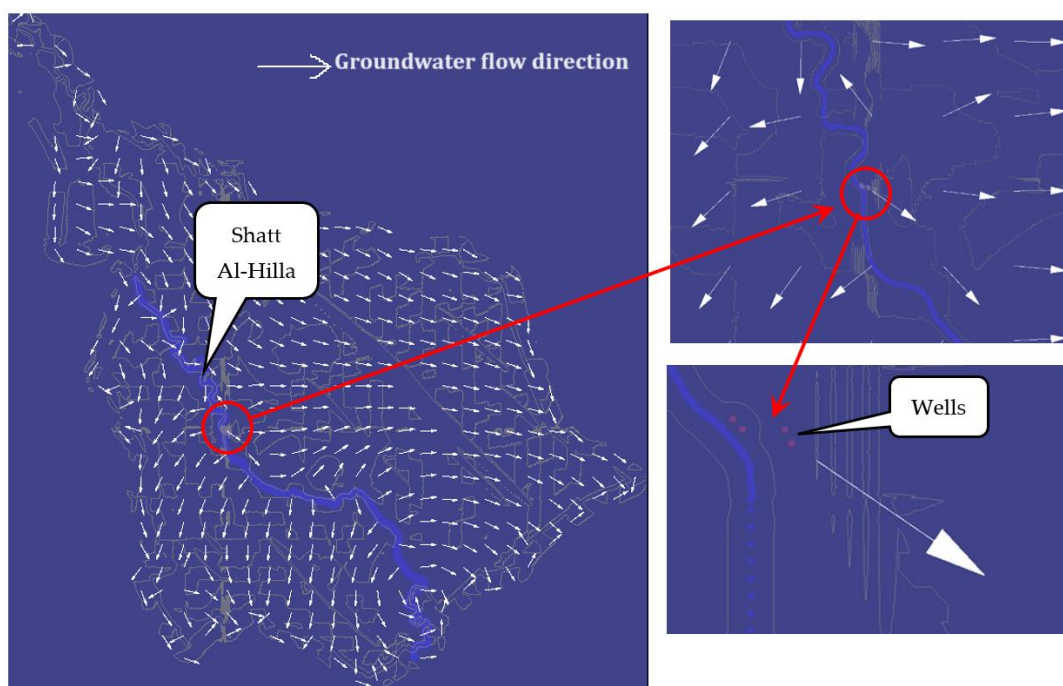


Figure 12. Seepage velocity direction maps.

Around the wells of the system, on a microscale, the reinjected water seeps equally in all directions. In the north and west directions of each well in the system, the reinjected water reverses the regional groundwater flow (from northwest to southeast), while in the east and south, the reinjected water boosts the regional groundwater flow, increasing the seepage velocity rate in these directions.

Regarding the magnitude of the seepage velocity, Figures 6–11 shows that the influence of ambient groundwater flow velocity on the thermal plume of the system is negligible. Bloemendal and Olsthoorn stated that regional groundwater flow velocities larger than 6.8 cm/d cause thermal losses [34]. Bloemendal and Hartog showed that systems with low ambient groundwater flow velocity (less than 6 m/year) have high storage efficiency values (greater than 80%) [34]. Al-Madhloom et al. (2020) determined the magnitude of the seepage velocity within the study area. According to their study, the magnitude of seepage velocity around the wells is limited to 5.09 mm/d [20]. All of these studies agree with the findings of this study regarding the negligible influence of ambient groundwater flow velocity on the system.

4. Conclusions

This paper considered two hydrogeological parameters that affect ATES system efficiency: the velocity of regional groundwater flow and neighbouring rivers.

In terms of regional groundwater flow, the ambient groundwater velocity that is available in the region of the system is limited to 5.09 mm/d. This velocity has a negligible influence on the thermal storage since the stored energy values are symmetrical under different conditions.

On the other hand, the influence of the neighbouring river (e.g., the Shatt Al-Hilla River) on the storage system can be well predicted by a simulation by adjusting the distance between the system and the river. In this study, two distances (75 m and 300 m from the river) were used to explore the influence of the neighbouring river. It was found that, when the system is about 75 m from the river, there are losses (leaks) from the stored energy to the river, while these losses did not appear when the system was placed 300 m from the river. Based on this finding, it can be concluded that (under the available hydrogeological conditions) a safe distance for constructing this type of storage system is 300 m from the river. This conclusion is valid for this type of storage system even at twenty years of operation.

The thermal gradient (especially for the second layer) increases with the time of operation due to the recharging of the system and the progression of the thermal waves (Figures 6–11). In addition, there is a considerable difference in the thermal gradient values between 10 m³/d on the one hand and 50 m³/d and 100 m³/d on the other. Accordingly, the thermal losses are much higher for flow rates of 50 m³/d and 100 m³/d than for the 10 m³/d flow rate.

Focusing on the middle layer, the spread of stored thermal energy (thermal plume) in it (storage layer) is very high compared to the other two layers (surface and lower). The reason for this is the high hydraulic conductivity of this layer compared to the other two layers.

By the end of the first year of operation, the temperature of the well cell almost reaches the temperature of the pumped water (36 °C for the warm well and 12 °C for the cold well), except when the flow rate is 10 m³/d.

We recommended that more studies explore surface thermal losses from ATES systems; the interaction of two or more neighbouring systems in the study area; and the design of a complex ATES system which consists of a group of warm wells and a group of cold wells. Also, more studies should be performed on the feasibility of implementing district aquifer thermal energy storage systems.

Author Contributions: Conceptualization, Q.H.M.A.-M.; methodology, Q.H.M.A.-M. and S.A.J.; software, Q.H.M.A.-M.; validation, Q.H.M.A.-M. and R.H.M.M.; formal analysis, Q.H.M.A.-M., S.A.J. and R.H.M.M.; investigation, Q.H.M.A.-M. and S.A.J.; resources, Q.H.M.A.-M. and R.H.M.M.; data curation, Q.H.M.A.-M., S.A.J. and R.H.M.M.; writing—original draft preparation, Q.H.M.A.-M.; writing—review and editing, Q.H.M.A.-M., S.A.J. and R.H.M.M.; visualization, Q.H.M.A.-M., S.A.J. and R.H.M.M.; supervision, Q.H.M.A.-M. All authors have read and agreed to the published version of the manuscript.

Funding: This research received no external funding.

Data Availability Statement: Data are contained within the article.

Acknowledgments: The authors would like to thank Anthony Pavlik for his help.

Conflicts of Interest: The authors declare no conflicts of interest.

References

1. Climate Change: Atmospheric Carbon Dioxide. Available online: <https://www.climate.gov/news-features/understanding-climate/climate-change-atmospheric-carbon-dioxide> (accessed on 1 December 2023).
2. Total Energy Supply, 2020, Middle East. Available online: <https://www.iea.org/regions/middle-east> (accessed on 1 December 2023).

3. Tawfeeq, A.H.; Hayder, A.M.; Ali, A.H. The Essential factors to reduce energy consumption in Iraq. In Proceedings of the 3rd International Scientific Conference of Alkafeel University, Najaf, Iraq, 22–23 March 2021.
4. CO₂ Emissions (kt)—Iraq. Available online: <https://data.worldbank.org/indicator/EN.ATM.CO2E.KT?locations=IQ> (accessed on 1 December 2023).
5. Alva, C.A.; Gould, T.; Kim, T.Y.; Mackey, P.; McGlade, C.; Olejarnik, P.; Walton, M.A.; Wanner, B. *Iraq's Energy Sector: A Roadmap to a Brighter Future*; International Energy Agency: Paris, France, 2019; pp. 5–45.
6. Fleuchaus, P.; Schüppler, S.; Godschalk, B.; Bakema, G.; Blum, P. Performance analysis of aquifer thermal energy storage (ATES). *Renew. Energy* **2020**, *146*, 1536–1548. [[CrossRef](#)]
7. Stemmler, R.; Blum, P.; Schüppler, S.; Fleuchaus, P.; Limoges, M.; Bayer, P.; Menberg, K. Environmental impacts of aquifer thermal energy storage (ATES). *Renew. Sustain. Energy Rev.* **2021**, *151*, 111560. [[CrossRef](#)]
8. Yang, T.; Liu, W.; Kramer, G.J.; Sun, Q. Seasonal thermal energy storage: A techno-economic literature review. *Renew. Sustain. Energy Rev.* **2021**, *139*, 110732. [[CrossRef](#)]
9. Bloemendal, M.; Jaxa-Rozen, M.; Olsthoorn, T. Methods for planning of ATES systems. *Appl. Energy* **2018**, *216*, 534–557. [[CrossRef](#)]
10. Fleuchaus, P.; Godschalk, B.; Stober, I.; Blum, P. Worldwide application of aquifer thermal energy storage—A review. *Renew. Sustain. Energy Rev.* **2018**, *94*, 861–876. [[CrossRef](#)]
11. Schüppler, S.; Fleuchaus, P.; Blum, P. Techno-economic and environmental analysis of an Aquifer Thermal Energy Storage (ATES) in Germany. *Geotherm. Energy* **2019**, *7*, 11. [[CrossRef](#)]
12. Amiri Delouei, A.; Sajjadi, H.; Ahmadi, G. Ultrasonic vibration technology to improve the thermal performance of CPU water-cooling systems: Experimental investigation. *Water* **2022**, *14*, 4000. [[CrossRef](#)]
13. Bloemendal, M.; Olsthoorn, T.; Boons, F. How to achieve optimal and sustainable use of the subsurface for aquifer thermal energy storage. *Energy Policy* **2014**, *66*, 104–114. [[CrossRef](#)]
14. Birdsell, D.T.; Adams, B.M.; Saar, M.O. Minimum transmissivity and optimal well spacing and flow rate for high-temperature aquifer thermal energy storage. *Appl. Energy* **2021**, *289*, 116658. [[CrossRef](#)]
15. Bloemendal, M.; Olsthoorn, T. ATES systems in aquifers with high ambient groundwater flow velocity. *Geothermics* **2018**, *75*, 81–92. [[CrossRef](#)]
16. Schmidt, T.; Pauschinger, T.; Sørensen, P.A.; Snijders, A.; Djebbar, R.; Boulter, R.; Thornton, J. Design aspects for large-scale pit and aquifer thermal energy storage for district heating and cooling. *Energy Procedia* **2018**, *149*, 585–594. [[CrossRef](#)]
17. Fakhari, M.; Raymond, J.; Martel, R.; Drolet, J.-P.; Dugdale, S.J.; Bergeron, N. Analysis of large-scale groundwater-driven cooling zones in rivers using thermal infrared imagery and radon measurements. *Water* **2023**, *15*, 873. [[CrossRef](#)]
18. Brielmann, H.; Griebler, C.; Schmidt, S.I.; Michel, R.; Lueders, T. Effects of thermal energy discharge on shallow groundwater ecosystems. *FEMS Microbiol. Ecol.* **2009**, *68*, 273–286. [[CrossRef](#)] [[PubMed](#)]
19. Bonte, M.; Stuyfzand, P.J.; Hulsmann, A.; Van Beelen, P. Underground thermal energy storage: Environmental risks and policy developments in the Netherlands and European Union. *Ecol. Soc.* **2011**, *16*, 22. [[CrossRef](#)]
20. Al-Madhlom, Q.; Al-Ansari, N.; Hamza, B.A.; Laue, J.; Hussain, H.M. Seepage velocity: Large scale mapping and the evaluation of two different aquifer conditions (silty clayey and sandy). *Hydrology* **2020**, *7*, 60. [[CrossRef](#)]
21. Yacoub, S.Y. Geomorphology of the Mesopotamia Plain. *Iraqi Bull. Geol. Min. (Spec. Issue)* **2011**, *4*, 7–32.
22. Yacoub, S.Y. Stratigraphy of the Mesopotamia Plain. *Iraqi Bull. Geol. Min. (Spec. Issue)* **2011**, *4*, 47–82.
23. Al-Jiburi, H.K.; Al-Basrawi, N.H. Hydrogeology of the Mesopotamia plain. *Iraqi Bull. Geol. Min.* **2011**, *4*, 83–103.
24. Al-Jiburi, H.K.; Al-Basrawi, N.H. Hydrogeological map of Iraq, scale 1: 1000 000, 2013. *Iraqi Bull. Geol. Min.* **2015**, *11*, 17–26.
25. Alwan, I.A.; Karim, H.H.; Aziz, N.A. Agro-climatic zones (ACZ) using climate satellite data in Iraq Republic. In Proceeding of the 2nd International Conference on Sustainable Engineering Techniques, Baghdad, Iraq, 6–7 March 2019.
26. Tabari, H.; Willems, P. Seasonally varying footprint of climate change on precipitation in the Middle East. *Sci. Rep.* **2018**, *8*, 4435. [[CrossRef](#)]
27. Kim, J.; Park, Y.; Harmon, T.C. Real-time model parameter estimation for analyzing transport in porous media. *Groundw. Monit. Remediat.* **2005**, *25*, 78–86. [[CrossRef](#)]
28. Zheng, C.; Wang, P.P. *MT3DMS: A Modular Three-Dimensional Multispecies Transport Model for Simulation of Advection, Dispersion, and Chemical Reactions of Contaminants in Groundwater Systems*; Documentation and User's Guide; US Army Corps of Engineers: Washington, DC, USA, 1999.
29. Bakr, M.; Van Oostrom, N.; Sommer, W. Efficiency of and interference among multiple aquifer thermal energy storage systems; A Dutch case study. *Renew. Energy* **2013**, *60*, 53–62. [[CrossRef](#)]
30. Al-Dabbas, M.; Al-Jabbari, M. Geometric properties of the River Euphrates, Iraq: The nature of its slope variation. In Proceedings of the Sediment Dynamics and the Hydromorphology of Fluvial Systems, Dundee, UK, 3–7 July 2006.
31. AL-Abbas, R.; Hommadi, A.; Abbas, A.; Essa, H.; Nheir, A. Checking the safety of Alhindya barrage foundation from uplift pressure and seepage ratio with variation of discharge and water level. In Proceeding of the International Conference on Civil and Environmental Engineering Technology, Al-Najaf, Iraq, 23–24 April 2019.
32. Jasim, N. Estimation of sediments transport of Euphrates River branches within Babylon city using a mathematical model. *J. Eng. Sci. Technol.* **2020**, *15*, 2163–2177.

33. Rahi, K.; Halihan, T. Changes in the salinity of the Euphrates River system in Iraq. *Reg. Environ. Change* **2010**, *10*, 27–35. [[CrossRef](#)]
34. Bloemendal, M.; Hartog, N. Analysis of the impact of storage conditions on the thermal recovery efficiency of low-temperature ATEs systems. *Geothermics* **2018**, *71*, 306–319. [[CrossRef](#)]

Disclaimer/Publisher’s Note: The statements, opinions and data contained in all publications are solely those of the individual author(s) and contributor(s) and not of MDPI and/or the editor(s). MDPI and/or the editor(s) disclaim responsibility for any injury to people or property resulting from any ideas, methods, instructions or products referred to in the content.